A quantitative inventory of yeast P body proteins reveals principles of composition and specificity

Wenmin Xing[1], Denise Muhlrad[2], Roy Parker[2], Michael K. Rosen[1]

[1]Department of Biophysics, Howard Hughes Medical Institute, UT Southwestern Medical Center, Dallas, TX, 79390

[2]Department of Biochemistry, Howard Hughes Medical Institute, University of Colorado, Boulder, CO, 80309

Corresponding author: michael.rosen@utsouthwestern.edu (M.K.R.)

ABSTRACT

P bodies are archetypal biomolecular condensates that concentrate proteins and RNA without a surrounding membrane. While dozens of P body proteins are known, the concentrations of components in the compartment have not been measured. We used live cell imaging to generate a quantitative inventory of the major proteins in yeast P bodies. Only 7 proteins are highly concentrated in P bodies (5.1-15 uM); the 24 others examined are appreciably lower (most ≤ 2.6 uM). P body concentration correlates inversely with cytoplasmic exchange rate. Sequence elements driving Dcp2 concentration into P bodies are distributed across the protein and act cooperatively. Our data indicate that P bodies, and probably other condensates, are biochemically simpler than suggested by proteomic analyses, with implications for specificity, reconstitution and evolution.

Currently 124 words (limit = 150)

INTRODUCTION

Eukaryotic cells contain numerous compartments that concentrate specific sets of molecules without a surrounding membrane (Banani et al., 2017; Shin and Brangwynne, 2017). These structures, referred to as biomolecular condensates, are related to a variety of biological processes. Examples include cytoplasmic processing bodies (P bodies) associated with RNA metabolism (Decker and Parker, 2012); promyelocytic leukemia nuclear bodies (PML NBs) involved in transcription, DNA damage repair, and anti-viral responses (Lallemand-Breitenbach and de Thé, 2010); signaling clusters in T cell activation (Su et al., 2016); and HP1 clusters in heterochromatin organization (Larson et al., 2017; Strom et al., 2017). Many condensates form through self-assembly of multivalent molecules, including proteins composed of folded domains and/or disordered regions, RNA and DNA, and chromatin (Li et al., 2012; Kato et al., 2012; Nott et al.,2015; Su et al., 2016; Banani et al., 2017; Gibson et al., 2019). This process can lead to both liquid-like and solid-like structures (Banani et al., 2017; Shin and Brangwynne, 2017; Alberti and Dormann, 2019). Some condensates have been shown to respond sharply to changes in concentration of key components or regulators, salt and/or temperature, suggesting that they form through highly cooperative assembly mechanisms, including phase transitions (Beutel et al., 2019; Brangwynne et al, 2009; Falahati and Wieschaus, 2017; Li et al., 2012; Riback et al., 2017; Saha et al., 2016; Smith et al., 2016; Wang et al., 2014; Weber and Brangwynne et al., 2015;). The activities of biomolecular condensates are thought to derive from the assembly of specific collections of functionally related molecules into a unique physical environment. Thus, understanding condensates as chemical entities requires knowledge and understanding of their compositions.

Large scale proteomics studies have been performed to determine comprehensive inventories of molecules that localize to different condensates, including stress granules (Jain et al., 2016; Markmiller et al., 2018; Youn et al., 2018), P bodies (Hubstenberger et al., 2017; Youn et al., 2018), and nucleoli (Anderson et al., 2002). There are also extensive studies on the localization of individual molecules to different condensates. Cumulatively, these studies suggest that condensates are biochemically complex, containing tens to hundreds of types of proteins and RNAs that show dense and complex

patterns of molecular interactions. Although some transcriptomic studies and a few analyses of individual proteins have been quantitative (Khong et al., 2017; Klingauf et al., 2006; Leung et al., 2006; Wheeler et al., 2017), proteomic studies to date have been only qualitative. Therefore both the relative and absolute concentrations of proteins in condensates, and their relationships to molecular connectivity, are largely unknown. Additionally, the relationships between concentration and dynamics of molecules in condensates have not been systematically explored. Moreover, while some components are shared between different condensates, many are uniquely concentrated in specific condensates. It is still unclear how the substantial specificity is determined *in vivo*.

To address these issues, we sought to examine the composition of a complex cellular condensate in a quantitative manner. We performed a systematic analysis of yeast P bodies, an archetypical biomolecular condensate. P bodies are protein- and mRNA-rich cytoplasmic condensates conserved from yeast to mammals (Ingelfinger et al., 2002; Sheth and Parker, 2003; van Dijk et al., 2002). They are thought to participate in RNA metabolism, modulating mRNA decay and acting as sites of RNA storage during cellular stress (Aizer et al., 2014; Bhattacharyya et al., 2006; Cougot et al., 2004; Sheth and Parker, 2003). Taking advantage of an available yeast GFP library, we used quantitative fluorescence microscopy to measure the absolute concentrations of 31 P body resident proteins within the condensates and in the surrounding cytoplasm. We also measured their dynamic properties using fluorescence recovery after photobleaching (FRAP). We find that P body proteins segregate into two groups based on their concentrations in P bodies and dynamics. Members of the first group (Dcp2, Edc3, Pat1, Xrn1, Lsm1, Dhh1, Upf1) are highly concentrated in P bodies (5.1-15uM) and exchange slowly with the cytoplasm. Except for Xrn1, these all have high connectivity, interacting with multiple P body components. Partitioning of several of these core proteins (Dcp2, Edc3, Pat1, and Xrn1) into P bodies is correlated, suggesting that they assemble cooperatively, consistent with their high connectivity. All proteins known to contribute strongly to P body formation through genetic studies are in this core group. In contrast, members of the second group are substantially less concentrated in P bodies (all except Sbp1, 0.7-2.6uM) and exhibit faster dynamics. These all have low connectivity. In a molecular dissection of Dcp2, we

find that the N-terminal domain, multivalent C-terminal domain, and central high affinity Edc3 binding site all contribute to partitioning of the protein into P bodies and to its dynamic exchange with the cytoplasm. Moreover, the N-terminal and C-terminal domains can act cooperatively to promote recruitment of Dcp2 into P bodies. This highly distributive organization suggests a ready means of quantitatively modulating condensate composition during evolution. These data suggest that while a condensate may contain many components, only a small number are highly concentrated there.

RESULTS

Strategies for quantification of P body proteins

In order to understand the chemical nature of a condensate it is important to both know its members, and also their concentrations. Two criteria must be met to accurately measure protein concentrations in a condensate based on fluorescence intensities alone: 1) the size of the condensate must be larger than the point spread function (PSF, i.e. the diffraction limit) of the microscope used in the analysis since the fluorescence intensities are diluted for small objects (Fink et al., 1998); 2) the composition of the condensate cannot change over time, allowing reliable comparisons among multiple condensates in multiple cells. P bodies in wild type *S. cerevisiae* are typically diffraction-limited in size under normal conditions. But they become larger when mRNA decay is decreased, e.g. when mRNA decay proteins such as Dcp1 are deleted or when cells respond to stresses such as glucose starvation (Teixeira et al., 2005, 2007). Initially we analyzed GFP-tagged proteins expressed in a *dcp1Δ* strain, because the effects of stress are time-dependent and thus more difficult to perform systematically measurements across a series of strains. We individually expressed 31 reported P body resident proteins tagged with GFP at their C-termini in their chromosomal location under their endogenous promoters (Figure 1 – figure supplement 1A, and Table 1). We presume these puncta are P bodies because previous reports that the proteins localize to P bodies and in all cases tested we observed co-localization of the proteins with an mCherry-tagged P body marker, Edc3 (Figure 1 – figure supplement 1B).

Using confocal microscopy, we limited our analyses to P bodies that were larger than the

x-y PSF of our microscope (see Methods), and corrected the diluting effect of the larger z-PSF based on an assumption that the structures were spherical. For each protein, we measured the absolute concentration in the P body and in the surrounding cytoplasm, based on cellular fluorescence intensity and independent calibration of fluorescence versus GFP concentration on our microscope (Figure 1 – figure supplement 2)(see details in Methods). We calculated the partition coefficient (PC) as the ratio of these two values.

We also used fluorescence recovery after photobleaching (FRAP) to measure the exchange between P bodies and the cytoplasm. Of the 31 proteins, 19 showed sufficiently punctate distributions in mid-log phase to permit analysis (PC > ~2). We refer to these 19 proteins as regular P body proteins hereafter. The remaining 12 proteins were distributed relatively uniformly in the cytoplasm and their P body concentrations could not be analyzed; these may be stress or strain specific proteins that do not concentrate in P bodies under our experimental conditions (Table 1).

Two observations suggest that the GFP tag probably does not strongly affect protein behaviors. First, the PC values and dynamics of Edc3 and Dhh1 tagged with GFP and mCherry were similar (Figure 1 – figure supplement 3A and 3B). Second, the PC values and dynamics of Dcp2 are nearly identical with an N-terminal or C-terminal GFP tag (Figure 1 – figure supplement 3C). In a screen of this size it is not practical to validate each protein with multiple tags at multiple locations. It remains possible that some other proteins are affected by the tag.

Seven proteins/assemblies are highly concentrated in P bodies

We obtained PC for all 19 regular P body proteins, which revealed subclasses of these molecules. Average PC values of the 19 regular P body proteins had a wide range, with a maximum of 133 (Dcp2) steadily decreasing to a minimum of ~5 (Eap1, Ssd1) (Figure 1A and Table 2). Only a few proteins had high partition coefficients, including Dcp2 (133 ± 13), Edc3 (133 ± 8) and Pat1 (107 ± 12); the majority had PC values <20. We also obtained absolute concentrations of each protein in P bodies, which ranged from ~0.7 uM to 15 uM and revealed two notable features of P bodies. First, seven proteins, Dcp2,

Edc3, Pat1, Xrn1, Lsm1 (likely representing the entire, constitutive Lsm1-7 assembly (Sharif and Conti, 2013)), Dhh1 and Upf1 – had average P body concentrations of 8.9 – 12 uM, with a slightly higher concentration (15 uM) for Dcp2 and slightly lower concentration (5 uM) for Upf1. We refer to these components as core P body proteins.

A second striking observation was that there was a clear, sharp distinction between highly concentrated and less concentrated proteins (Figure 1B). After the core proteins most other proteins have P body concentrations < 2.6 uM, with most ~1 uM. The only exceptions is Sbp1 (4.6 uM), which also has a very high cytoplasmic concentration, affording it a high P body concentration even with a small PC value (Figure 1, and Table 2). Sbp1 also is not highly enriched in glucose-starved wild type P bodies (see below); for these reasons we do not include it in the core group. Our data are consistent with previously reported measurements since the total cellular concentrations that we measured are similar to a unified quantitative protein abundance database of *S. cerevisiae* (Ho et al., 2018) (Figure 1 – figure supplement 3D).

Together, these data show that while yeast P bodies can contain many different proteins, only a relatively small number are highly concentrated in the compartment, and the majority of components are weakly concentrated.

Core proteins tend to have slow dynamics

We also examined the dynamics of the 19 regular P body proteins using FRAP. For each GFP-fusion expressing strain, entire P bodies (0.4 - 0.8 um) were photobleached and the fluorescence recovery curves were fit to single exponential. The exchange rate (k) and fractional recovery were used to assess their dynamics. This analysis revealed that the regular P body proteins exchange with the cytoplasm with very different rates and fractional recoveries (Figure 2 – figure supplement 1 and Table 2). At one end of the distribution, Dcp2 and Edc3 showed no measurable recovery on a 150 second timescale. Proteins such as Pat1 and Upf1, showed intermediate rates and extents of recovery (k = ~0.01 s^{-1}, recovery = ~50%). While at the other end of the spectrum, proteins such as Sbp1 and Eap1 recovered nearly 100% in 150 s (k =0.07 s^{-1}).

Since we observed heterogeneity of both partitioning and dynamics, we asked whether these parameters are related. For each protein, we plotted the exchange rate (*k)*, and fractional recovery against P body concentration (Figure 2A and 2B). Although exchange rate and recovery for both core proteins and non-core proteins spanned broad ranges, the core proteins (Dcp2, Edc3, Pat1, Xrn1, Lsm1, Upf1, and Dhh1) tended to have slower exchange rates and less fractional recoveries than the non-core proteins (Figure 2A and 2B). On average, for the core group, the exchange rate was five-fold smaller than the non-core group, and recovery fraction was two-fold lower (Figure 2A and 2B).

Three observations argue that the slower recovery dynamics of the core proteins are not simply due to smaller fluorescent pools in cytoplasm, but rather reflect different interactions in the P body. First, neither exchange rate nor fractional recovery correlates with protein concentrations in cytoplasm (Figure 2 – figure supplement 2A and 2B). Second, less than 50% of the total pool of each protein is localized to the P body (< 8% for most), suggesting that there are still substantial fluorescent pools in the cytoplasm (Figure 4). Third, we also performed inverse FRAP (iFRAP), which is insensitive to the size of fluorescent pools, for several proteins. In iFRAP, the entire cytoplasm except one P body was bleached and the loss of fluorescence in the P body was followed over time. In each case, the exchange rate and fractional recovery measured by iFRAP was similar to those measured by FRAP (Figure 2 – figure supplement 2C and 2D).

Partitioning of core proteins into P bodies is correlated

We noticed that the PC values and P body concentrations of proteins varied in a broad range, for example, the PC of Dcp2 varied from 50 to 250 between different cells (Figure 1). In addition, the core proteins, Dcp2:Edc3:Pat1:Lsm1:Dhh1:Xrn1, are present at roughly equimolar average levels (~10 uM), suggesting their concentrations may be correlated. To better understand the variability of partitioning, we measured the concentrations of pairs of core proteins, differentially tagged with GFP or mCherry, in the same P bodies (Figure 3A). This revealed that the concentrations of paired Edc3 and Dcp2, Pat1 and Dcp2, and Xrn1 and Dcp2, are positively correlated as indicated by

Pearson correlation coefficients of 0.6 – 0.7 (Figure 3B, 3C, and 3D). Moreover, the ratios of the two measured protein concentrations have narrower ranges than the ratios calculated by randomizing the pairing (Figure 3A and 3E). These data indicate that partitioning of core proteins into P bodies is correlated, suggesting they assemble cooperatively (see Discussion).

Partitioning and dynamics of proteins are not strongly affected by Dcp1 deletion

Since the above analysis was all performed in a *dcp1*Δ strain, we wanted to measure PC and P body dynamics under a different condition to evaluate if the Dcp1 deletion made a substantial impact on P body composition or dynamics. For this experiment, we analyzed wild type strains after 30-60 min of glucose starvation. By several criteria, we observed similar results to our analysis in *dcp1*Δ strains.

First, similar to the *dcp1*Δ strains, during glucose deprivation, Dcp2, Edc3, Pat1, Lsm1, Xrn1, Upf1, and Dhh1, remain the most concentrated proteins in wild type P bodies, although Pat1 and Lsm1 dropped compared to the *dcp1*Δ strains (Figure 1 – figure supplement 4A and 4B). Two additional proteins, Dcp1 and Pby1, also partition strongly into wild type P bodies under glucose starvation. Dcp1 binds with high affinity to Dcp2, and Pby1, in turn, binds to Dcp1, explaining its absence in *dcp1Δ* P bodies (Krogan et al., 2006). Only two members of the non-core group, Hek2 and Sbp1, partition sufficiently to permit analysis suggesting that the partitioning of non-core proteins is lower under glucose starvation.

We also observed that the dynamics of all proteins under glucose starvation were qualitatively similar to the *dcp1Δ* strains. The core proteins have slower dynamics, although there is no clear distinction between core and non-core groups because of the limited number of the latter (Figure 1 – figure supplement 4C and 4D). Nevertheless, these data suggest that partitioning and dynamics of proteins are qualitatively similar in the wild type strains under glucose starvation and the *dcp1Δ* strains, especially for the core proteins. We thus performed all subsequent experiments in *dcp1Δ* strains, unless stated otherwise.

P bodies not strongly sequester their resident proteins

The biological importance of concentrating certain proteins into P bodies is unclear. One proposed function is that the P body could sequester molecules, inhibiting their activities in the cytoplasm. Similarly, P bodies have been suggested to store mRNAs or proteins under cellular stress, which could then be returned to the cytoplasm when the stress is resolved (Aizer et al., 2014; Bhattacharyya et al., 2006). To examine the efficiency of protein sequestration, we quantified the fractions of each P body protein in the compartments (F_P). We first measured F_P in mid-log phase without stress. Under these conditions, the most concentrated proteins, Dcp2 and Edc3, are on average ~30% sequestered in observable P bodies (Figure 4). For the other highly concentrated proteins (Pat1, Xrn1, Lsm1, Upf1, and Dhh1), about 10% is sequestered in visible P bodies. F_P is even smaller for less concentrated proteins such that only about 5% of each is in visible P bodies.

We further asked if the degree of P body sequestration in *dcp1Δ* strains increases under glucose starvation (Teixeira and Parker, 2007). Thus, we measured F_P after 4h of glucose starvation. Although F_P increased for most of the proteins, visible P bodies still sequester less than 40% of each of the concentrated proteins (Figure 4 – figure supplement 1A). We next grew cells to stationary phase to test if P bodies convert to sequestration sites at different growth stages. Again, less than 50% of each protein except Dcp2 and Edc3 is in P bodies (Figure 4 – figure supplement 1B).

One possible explanation for the low degree of sequestration is that many P bodies are too small to be observed by standard confocal microscopy (Rao and Parker, 2017). This would give artifactually low F_P values, as a significant fraction of P body-associated protein would not be accounted for in the integrated P body fluorescence intensity. Nevertheless, we can estimate an upper limit of F_P for most proteins by assuming that all P bodies in a given cell have identical compositions independent of size, and that the F_P value for the most sequestered protein (Dcp2), is, in fact 1 when small P bodies are properly accounted for. With this assumption, the estimated maximum F_P ($F_{P,max}$) for each

protein would be $F_{P,max} = F_P * 1/ F_{P(Dcp2)}$. Even with this conservative estimate, most proteins are only sequestered to < 20% in P bodies under all conditions.

Together, our quantifications indicate that P bodies do not strongly sequester their resident proteins under the conditions examined. Our data of course do not rule out the possibility that sequestration could be higher under different conditions, nor do they speak to sequestration/storage of RNA, which could have even higher PC values than proteins, perhaps due to non-equilibrium processes (Ditlev et al., 2018; Hubstenberger et al., 2017).

Elements controlling Dcp2 partitioning and dynamics are distributed across the protein

We have shown that proteins concentrate into P bodies to different degrees and with distinct dynamic behaviors. We next sought to understand what molecular features could control these properties, using Dcp2, one of the most highly concentrated and least dynamic P body components, as an example. We divided Dcp2 into three distinct regions (Figure 5A). The N-terminal domain (NTD) of the protein possesses decapping activity and binds to Dcp1 and mRNAs (Deshmukh et al., 2008; She et al., 2008). The multivalent C-terminal domain (CTD) contains multiple short helical leucine rich motifs (HLMs) that bind to Edc3. Finally, near the center of Dcp2, the first HLM (HLM1) appears to bind Edc3 with appreciably higher affinity than all other HLMs (Charenton et al., 2016), and mutations to this motif impair Dcp2 partitioning into P bodies (Harigaya et al., 2010). We expressed different Dcp2 variants in *dcp1Δdcp2Δ* strains, in which P bodies are still formed (Figure 5 – figure supplement 1A), but they are smaller than in yeast expressing full length Dcp2. The expression levels of these Dcp2 variants are similar to wild type Dcp2 as assessed by western blotting (Figure 5 -– figure supplement 1B). The analysis of these variants identified three molecular elements of Dcp2 that affect its partitioning into P bodies.

First, we found that N-terminally truncated Dcp2 (Dcp2ΔN) partitions into P bodies less efficiently than the full-length protein (Dcp2 FL), with PC values of 72 ± 8 and 124 ± 9, respectively. FRAP analysis revealed that Dcp2ΔN had an appreciably higher recovery

fraction, 0.35 over 150 seconds, compared to Dcp2 FL, which does not recover at all in this timeframe (Figure 5B and 5C). This demonstrates that the N-terminal domain of Dcp2 promotes P body accumulation.

Second, mutating HLM1 (Dcp2ΔH1) to alanine in the full-length protein strongly decreased the PC to ~26, and increased the recovery after photobleaching to 0.65 over 150 seconds. Thus, both the NTD and HLM1 contribute to concentrating Dcp2 into P bodies and decreasing its exchange with the cytoplasm.

Third, additional data suggest that the other HLMs in Dcp2's C-terminal extension can contribute to P body targeting when HLM1 is missing. This is based on the observations that while truncation of the CTD (Dcp2 300) had no significant effect on the PC and dynamics of Dcp2 (Figure 5B and 5C), removing the C-terminal domain from Dcp2 ΔH1 (Dcp2 300ΔH1) impaired recruitment to P bodies (Figure 5D).

Since the N-terminal domain, HLM1, and C-terminal domain are all required for efficient partitioning and maintaining the characteristic slow dynamics of Dcp2, we conclude that elements controlling protein partitioning and dynamics are distributed across the protein.

Recruitment elements of Dcp2 act cooperatively

We next asked whether these regions can act cooperatively to promote P body recruitment. We analyzed three Dcp2 mutant fragments in *dcp1Δdcp2Δ* strains: 1) Dcp2 300ΔH1, which can only interact with RNA; 2) a C-terminal Dcp2 fragment, Dcp2C Δ5H, in which five out of nine HLMs have been inactivated by mutations to further impair partitioning into P bodies. This construct should not bind RNA, and only interact with Edc3 weakly since it is missing the high affinity H1 site; and 3) Dcp2ΔH1 Δ5H, fusion of Dcp2 300ΔH1 and Dcp2C Δ5H, which interacts with both RNA and Edc3 (Figure 5A and 5G). The three mutants expressed at similar levels in *dcp1Δdcp2Δ* strains (Figure 5 – figure supplement 1C). We analyzed recruitment of the three proteins into P bodies using Edc3 as a P body marker.

We observed synergistic effects between these two regions of Dcp2. Specifically, Dcp2 300ΔH1 and Dcp2C Δ5H are measurably recruited into microscopic P bodies in only ~20% and ~30% of cells, respectively. However, the fusion of the two fragments, Dcp2ΔH1 Δ5H, is recruited into P bodies in ~95 % of cells (Figure 5D and Figure 5E). Moreover, partition coefficients of Dcp2 300ΔH1 and Dcp2C Δ5H are 2.5 and 3.5, respectively, while the partition coefficient of Dcp2ΔH1 Δ5H is 31 (Figure 5E). Since the product of the individual partition coefficients (8.75, which is exponentially related to the sum of the free energies of partitioning) is less than that of the fusion protein (31), we conclude that the elements act cooperatively in the fusion to promote accumulation into P bodies.

Thus, while Dcp2 300ΔH1 and Dcp2C Δ5H are each recruited only weakly to P bodies, their fusion, Dcp2ΔH1 Δ5H, is recruited strongly. This indicates that recruitment elements can act cooperatively when fused in cis, even when they recognize distinct ligands (in this case, Edc3 and RNA) within a condensate (Figure 5G).

Partitioning of Dcp2 into P bodies can be saturated

Our data also indicate that although elements controlling partitioning are distributed across Dcp2, their efficiencies are not equal (Figure 5). For example, deleting the NTD causes a 40% decrease in PC (Dcp2 FL vs Dcp2ΔN) while deleting HLM1 causes an 80% decrease (Dcp2 FL vs Dcp2ΔH1) (Figure 4A, and 4B). Further, deleting the CTD has no effect on PC of full length Dcp2 (Dcp2 FL vs Dcp2 300, Figure 4A, and 4B), while deleting the CTD in the background of an HLM1 deletion causes a 10-fold decrease in PC (Dcp2ΔH1 vs Dcp2 300ΔH1, Figure 4A, 4B, and 4C). To further examine this issue, we added HLM1 to Dcp2FL and DcpC Δ5H, referring to these variants as Dcp2FL-H1, and DcpC Δ5H-H1, respectively (Figure 6A). For the weakly partitioning DcpCΔ5H, adding HLM1 significantly increased its concentration in P bodies to ~16uM, comparable to Dcp2 FL, and increased its partition coefficient to ~69 (Figure 6B, 6C, and 6D), although Dcp2CΔ5H expressed higher than Dcp2CΔ5H-H1 (Figure 6 – figure supplement 1). In contrast, adding HLM1 to Dcp2 FL, which already partitions into P bodies strongly, does not significantly further enhance either the absolute concentration or partition coefficient.

Thus, binding of HLM1 to Edc3 can contribute strongly to Dcp2 partitioning. However, the interaction between the two wild type proteins appears to be effectively saturated, consistent with their strong correlation in concentrations in P-bodies (Figure 3), and increasing their affinity by adding a second HLM1 element to Dcp2 does not draw more of the protein into P bodies. In general, while partitioning into a condensate can be increased by strengthening weak interactions between a pair of components, the magnitude of such an effect is limited as binding nears saturation.

RNA binding and turnover affect Dcp2 partitioning and dynamics

As the N-terminal domain of Dcp2 possesses both RNA binding and decapping activities, we further asked how these two interactions with RNA, an important scaffold of P bodies, affect partitioning and dynamics. Starting with the Dcp2 300 fragment, we mutated previously reported RNA binding residues, R170, K212, K216, and R229, to alanine, generating Dcp2 300 AAAA (Figure 7A) (Deshmukh et al., 2008). Dcp2 300 AAAA does not partition into P bodies, despite being expressed similarly to Dcp2 300 (Figure 7 – figure supplement 1A), suggesting that RNA binding is important for Dcp2 partitioning (Figure 7B).

To investigate the effect of catalytic activity on Dcp2 partitioning and dynamics, we made mutations in the Dcp2ΔH1 construct, affording a better dynamic range than the wild type protein (Figure 5B). We mutated W50 and D54, which were previously implicated in RNA cap recognition and hydrolysis, to alanine, giving Dcp2ΔH1 WD (Figure 7A) (Charenton et al., 2016; Floor et al., 2010). We then analyzed Dcp2ΔH1 and Dcp2ΔH1 WD in a *dcp2Δ* strain, where the former protein should reconstitute significant mRNA decapping activity while the latter should not.

We observed that formation of P bodies was promoted by expressing Dcp2ΔH1 WD (Figure 7C), which is consistent with previous observations that mutations that block decapping catalysis lead to increased P bodies (Sheth and Parker, 2003; Teixeira and Parker, 2007). Dcp2ΔH1 WD formed six P bodies per cell on average, compared to two P bodies per cell for Dcp2ΔH1 (Figure 7D), despite being expressed at similar levels

(Figure 7 – figure supplement 1B). Changing the catalytic rate of decapping also changed the accumulation of Dcp2 in P bodies and altered its dynamics. Specifically, ~10% of Dcp2ΔH1 WD was concentrated in visible P bodies compared with ~4% for Dcp2 ΔH1 (Figure 7E). The exchange rate also decreased from 0.041 s^{-1} to 0.017 s^{-1} and fractional recovery decreased from 0.85 to 0.65 in the WD mutant (Figure 7F).

To further test whether these changes are due to increasing amounts of cellular mRNA or to disrupting catalytic activity of Dcp2 *per se*, we analyzed these two variants after 30-60 minutes of glucose starvation, conditions in which mRNA is increased due to translation repression. We observed that under these conditions Dcp2ΔH1 and Dcp2ΔH1 WD showed similar dynamics (exchange rates of 0.021 s^{-1} and 0.013 s^{-1}, respectively, and fractional recoveries of 0.57 and 0.60, respectively, Figure 7F) and a similar distribution of the number of P bodies per cell (Figure 7D), suggesting that the differences observed in the non-starved conditions were due to differences in mRNA concentration. However, even in the starved conditions, the Dcp2ΔH1 WD mutant still shows a larger total fraction in P bodies than the Dcp2ΔH1 protein (Figure 7E), indicating that catalytic activity does control some aspects of P body formation. Together these data suggest that changes in the partitioning and dynamics of the Dcp2 WD mutant are caused by a combination of increase mRNA concentration and loss of catalytic activity.

DISCUSSION

This work presents the first quantitative description of an RNP granule, which is representative of the broader class of non-membrane bound organelles referred to as biomolecular condensates. This analysis has exposed features of yeast P bodies that should be generalizable to other condensates.

Two classes of P body components

A major contribution of this work is to demonstrate two distinct classes of proteins within yeast P bodies. Members of one class, which we name the core P body proteins, are highly enriched, with PC ≥ 30 and P body concentrations > 5 uM. These include Dcp2, Edc3, Pat1, the Lsm1-7 complex, Xrn1, Dhh1, and Upf1 (colored red in Figure 1). On

average, these proteins show slower dynamics of exchange from P bodies and a small fraction of exchangeable molecules. In contrast, the non-core P body proteins, Not2, CCR4, Pop2, Upf2, Upf3, Hek2, Eap1, Edc1, Bre5, Psp2, Sbp1 and Ssd1, have PC < 15, lower concentrations in P bodies, and show rapid exchange with the cytoplasm and a large fraction of exchangeable molecules. Thus, despite their apparent complexity from the literature, yeast P bodies are made up of a core group of proteins at high concentrations, with much lower concentrations of additional factors. This illustrates a likely general principle that biological condensates that appear quite complex by qualitative analyses of their components, may in fact have a much simpler primary complexity and organization.

The differences between core and non-core P-body proteins are probably closely related to their intermolecular connectivity patterns within P bodies, which are listed in Table 3 based on literature data. With the exception of Xrn1 (see below), the core proteins all have high valency of interaction (number of interacting molecules) and high connectivity to other P body proteins and RNA (≥ 4 directly interacting molecules). This connectivity should afford increased partitioning into the condensate and reduced exchange rates and fractional recovery with the surrounding cytoplasm. It should also enhance the ability of the core proteins to assemble, and thus contribute significantly to P body formation. In contrast, all non-core proteins have low valency and low connectivity, and usually interact with RNA and/or only one core protein. These features should generally afford lower P body concentrations and more rapid and complete exchange. Since many of the non-core components are RNA binding proteins (Table 3 and Figure 2 – figure supplement 3), we suggest they are recruited into P bodies by the high local concentration of RNA. The non-core components with the highest PC (Pop2, Ccr4, Upf2, Upf3) all also have direct interactions with a core P body component (Pop2 interacting with Dhh1, Upf2 interacting with Upf1), consistent with the idea that partitioning is determined by cooperative interactions of a given protein with multiple components within a condensate (see below). Thus, connectivity, and its molecular underpinning, valency of interaction, is likely to provide significant predictive power in understanding the composition of condensates.

We note that while connectivity is significantly correlated with P body concentration and dynamics, the correlation is not perfect, likely because affinity and energy-consuming processes, in addition to connectivity, can play a significant role. For example, the PC of the 1-300 fragment of Dcp2, which includes the HLM1 high affinity binding site for Edc3, is 132. In contrast, the PC of the Dcp2ΔH1-H5Δ, where HLM1 is replaced by lower affinity binding sites for Edc3 in the C terminal extension of Dcp2, is only 31. Similarly, the core protein Xrn1 is concentrated in P bodies to ~10 uM even though it only has 2 connections to other P body components. This is presumably due to the high affinity of the protein for RNA (Chang et al., 2011; Banani et al., 2016). Finally, the exchange dynamics of Dhh1 appear to be governed by its rate of RNA-dependent ATP hydrolysis (Mugler et al., 2016). Thus, while connectivity patterns can be a useful guide to condensate composition and behavior, other molecular details must be considered to develop a complete understanding.

Assembly of P bodies through cooperative interactions

Our data also provide insights into the nature of P body assembly. The positive correlations between core protein concentrations (Figure 3) suggest that these molecules partition into P bodies cooperatively. This cooperativity likely arises from the high connectivity among the core proteins, such that partitioning of one molecule promotes partitioning of others that interact with it directly and indirectly. Given the high concentration and multivalency of core P-body components one would predict that they would all be able to contribute to P-body assembly. Indeed, this is what is seen in the literature. The three most enriched P body components, Dcp2, Pat1, and Edc3, are the three major proteins shown to affect P body assembly (Buchan et al., 2008; Decker et al., 2007; Teixeira and Parker, 2007). Other core proteins, Dhh1, Upf1, and the Lsm1-7 complex can contribute to P body assembly as well (Decker et al., 2007; Sheth and Parker, 2006; Hondele et al., 2019; Rao and Parker, 2017). In contrast, none of the non-core components are required for efficient P-body assembly. This illustrates a second principle that interactions that produce condensates are distributed across their highly-valent components. These act with differing degrees of cooperativity to promote formation of

the larger assembly. This principle can explain why smaller P-bodies can still assemble in cells lacking one core protein component (Rao and Parker, 2017).

It is notable that in the *dcp1Δ* strains, the core components, Dcp2:Edc3:Pat1:Lsm1:Dhh1:Xrn1, are present at roughly equimolar concentrations (~10 μM), with the exception of Upf1, which is ~2-fold lower. This suggests that perhaps these components form a discrete, stoichiometrically defined RNP complex which then assembles to higher order to form the condensate. However, our data speak against this extreme of high cooperativity. First, the ratio of Dcp2 to Edc3 ranges from 0.5 to 2.3 in our analysis, inconsistent with a strictly defined ratio expected from a stoichiometric complex on every mRNA. Cast differently, the cooperativity in P body concentrations illustrated in Figure 3 is significant, but not as high as expected from a discrete complex. Further, the P body concentrations of Pat1 and the Lsm1-7 complex drop about two fold in wild type strains under glucose starvation conditions relative to the *dcp1Δ* strains, again speaking against a discrete assembly and suggesting that the interaction network of the core proteins could be altered under different conditions.

An unanswered question is whether intermolecular RNA-RNA interactions contribute to P-body assembly. This possibility is suggested by the robust self-assembly of RNA, the roles of intermolecular RNA-RNA interactions in stress granule assembly (Van Treeck at el., 2018; Tauber et al., 2020), the observation that RNA is required for P body formation (Teixeira et al., 2005), and the fact that every P body protein interacts with RNA (Table 3 and Figure 2 – figure supplement 3). P-body formation clearly requires protein interactions since Dcp2, Edc3, Dhh1, Lsm1-7 complex and Pat1 have all been genetically shown to promote P-body formation (Decker et al., 2007; Teixeira and Parker, 2007; Rao and Parker, 2017; Hodele et al., 2019). In some cases, the assembly of P-bodies can be directly attributed to specific protein-protein interactions, such as the requirement for Edc3 dimerization to promote P-body formation (Ling et al., 2008). Moreover, several P-body proteins either in isolation, or in mixtures, can undergo LLPS to create P-body-like assemblies in vitro (Fromm et al., 2014; Schutz et al., 2017). Whether the mRNAs in P-bodies simply serve as a platform to facilitate interactions

between core P-body components, or also form intermolecular RNA-RNA interactions contributing to P-body formation remains to be seen.

General Principles of scaffolds and clients in natural condensates

We previously proposed that the components of biomolecular condensates could be classified into two groups, scaffolds and clients (Banani et al., 2016; Ditlev et al., 2018). Scaffolds are defined as components that are required for condensate formation, while clients are not necessary for integrity of the condensate, but are recruited by interacting with scaffolds. As corollaries, the model posited that there should generally be few scaffolds and many clients in natural condensates, and that scaffolds should have high valency of interaction elements, while clients should have lower valency. In addition, scaffolds should have higher concentration within the condensate than clients, since the former recruit the latter. The model was generated based largely on the behaviors of engineered multivalent macromolecules, where the distinction between scaffold and client was stark by design. In this view, the yeast P body scaffolds include RNA (Teixeira et al., 2005) as well as Dcp2, Edc3, and Pat1, Lsm1-7 and Dhh1 (Decker et al., 2007; Teixeira and Parker, 2007; Hondele et al., 2019), since deletion of these factors impairs formation of the condensate. Notably, all of these proteins are in the core group and have high valency of interaction and high connectivity. Under the same conditions, no molecules in the non-core group are known to impair P body formation (although when cells are at high density, deletion of Sbp1 produces smaller P bodies (Segal et al., 2006)). Thus, information on the relative concentrations of proteins in a condensate (the core vs non-core distinction) is likely to aid prediction of molecules that play significant roles in generating the structure (and be imperfectly correlated with connectivity, as described above).

Yet a simple scaffold/client classification does not account for the differences in effect of the various deletions; e.g. loss of RNA completely eliminates P bodies, whereas loss of the other factors has only a partial effect. Thus, rather than a black-and-white classification, we have come to believe that scaffold and client are better used as descriptors, where condensate components are more scaffold-like or more client-like depending on the degree to which their deletion affects the cooperative assembly of other

components. Scaffold-like components contribute more strongly to condensate formation; their deletion should decrease the size and number of condensates. Client-like components should have lesser or no such effects. In the context of phase transitions, the descriptor characterizes the degree by which a given condensate component influences the multi-dimensional phase boundary of the system, both the position of the boundary and its shape, since effects of deletion are unlikely to be evenly distributed across all molecules in a condensate (see below). Deletion of scaffold-like molecules will produce larger changes and deletion of client-like molecules will produce more subtle effects.

Intuitively, scaffold-like components should have higher connectivity among molecules in the condensate, and will be more central in the interaction network, whereas client-like molecules should have low connectivity and be more peripheral in the network. In addition to affecting formation of the condensate, highly connected molecules are expected to have greater influence on the composition of the structure. Deletion of scaffold-like molecules will change partitioning of numerous components, while deletion of client-like molecules will only affect partitioning of their immediate interacting components in the network. Importantly, since connectivity in a condensate is not homogeneous, deleting molecules is likely to have heterogeneous effects on composition, changing the relative ratios of components. Thus, the thermodynamics of forming a condensate and the composition of the resulting structure will be coupled, based on the connectivity patterns in the interaction network. Further exploration of these ideas will require large-scale, systematic analysis of condensate composition in the presence of individual deletions of multiple components.

Compositional specificity

A major question regarding biomolecular condensates is how the composition of the compartments is determined *in vivo*. Our data suggest that recruitment of Dcp2 into P bodies is distributed across a large number of interaction elements, including a high affinity Edc3-binding motif, an RNA binding domain and weak multivalent interactions with

Edc3. This organization provides several insights into compositional specificity that should be generalizable to other molecules.

First, simple mass action will concentrate components that bind with high affinity to scaffolds. For example, adding the high affinity HLM1 to the weakly partitioning Dcp2CΔ5H promotes its partitioning into P bodies to a level similar to that of wild type Dcp2. High affinity binding to RNA likely also explains the strong partitioning of Xrn1 into P bodies, even though it makes few known interactions with other components and its loss does not have deleterious effects to formation of the condensates (i.e. it is more client-like than scaffold-like in its properties).

Second, increasing affinity for a condensate component does not increase partitioning if affinity is already high. We found that adding a second HLM1 element to full length Dcp2, which should increase affinity for Edc3, does not increase its partition coefficient. The upper bound may be determined by limiting concentrations of scaffold-like interaction partners. This also indicates that partitioning may be more readily tuned when it is mediated by weak multivalent interactions rather than by high affinity interactions.

Third, protein elements that bind scaffold-like components weakly will not partition strongly into a condensate, but when two such elements are fused together, even if they bind different scaffold-like components, they can be recruited strongly. We found that two fragments of Dcp2, which bind RNA and Edc3, respectively, partition only weakly into P bodies individually. Yet when fused together, they are recruited strongly. This behavior is analogous to previous observations that cooperativity between IDRs and folded domains can promote recruitment into both phase separated droplets *in vitro* and P bodies in cells (Lin et al., 2015; Protter et al., 2018). The behavior likely is mechanistically similar to avidity effects in canonical molecular interactions, where high affinity can be achieved through multivalent binding. Such effects will greatly narrow the specificity of recruitment, even for scaffolds that individually bind ligands promiscuously. This mechanism also provides ready routes for evolution of new clients through genetic rearrangements that fuse together multiple low-affinity interaction elements. Distributing recruitment across a

large number of interaction elements would also render composition less susceptible to mutations, which could lead to evolutionary selection.

Quantitative considerations of condensate function

Quantitative analyses as we have performed play an important role in assessing the functions of condensates. For example, several condensates, including P bodies, have been proposed as sites for sequestration/storage of biomolecules, in part because they appear as qualitatively bright puncta by microscopy, and in part because their disruption can activate certain processes (Arimoto et al., 2008; Decker and Parker, 2012; Li et al., 2000). However, when total condensate volume (typically < 1-2 % of cytoplasm/nucleoplasm), and partition coefficients (2~200) are quantified, it is evident that only a small fraction of most molecular species are sequestered within condensates. (Figure 4, Leung et al., 2006; Rao and Parker, 2017; Wheeler et al., 2017). While in some processes small changes in the amount of available species in the cytoplasm/nucleoplasm could have functional consequences, in others, different mechanisms must be considered. For example, rather than sequestration, an inhibitory catalytic function within a condensate could also explain the activation of a process upon condensate disruption. Such considerations will further advance the already significant impact of biochemical reconstitutions of phase separation on understanding the functions of biomolecular condensates (Fromm et al., 2014; Schütz et al., 2017; Woodruff et al., 2017).

Conclusions

Together, our work suggest that condensates may generally be organized around a relatively small number of highly concentrated, less dynamic scaffold-like components. This construction would provide a relatively simple route for a condensate to appear during evolution, in that only a small number of proteins would need to develop the ability to assemble cooperatively. Once this structure was established, other proteins could evolve the ability to interact with the scaffold-like components and consequently be recruited into the compartment to different degrees determined by their connectivity, interaction affinity and cooperativity among different interaction elements. A composition

of this nature also indicates that condensates are biochemically less complicated than suggested by proteomics studies, where tens to hundreds of proteins have been annotated as residents of particular condensates. Our quantitation indicates that most components are present in only small amounts, and the majority of the protein mass derives from only a few types of molecules. Such an understanding greatly simplifies efforts to reconstitute condensates in vitro, and can frame models of their biochemical functions.

Materials and Methods

Yeast strains

Yeast strains used in this study are listed in Table 1. GFP or mCherry tagged proteins used to generate figure 1-4 are expressed from their endogenous locus. Yeast strains carrying plasmids were constructed using lithium acetate-based transformation (Gietz and Schiestl, 2007).

Plasmid construction

Plasmids used in this study are listed in Table 4. All Dcp2 mutants were expressed under the *DCP2* promoter on a low-copy centromeric plasmid (pRP1902) as previously reported (Harigaya et al., 2010). Dcp2 point mutations were made by site-directed mutagenesis using KOD Xtrem Hot start DNA Polymerase followed by Dpn1 digestion. Dcp2C Δ5H, and Dcp2 ΔH1 Δ5H were constructed by Gibson assembly into the vector used for Dcp2 FL, pRP1903 (Harigaya et al., 2010). N-Dcp2 was also constructed from pRP1903.

Yeast growth conditions

dcp1Δdcp2Δ strains and *dcp2Δ* strains expressing GFP tagged Dcp2 mutants were grown in synthetic medium lacking uracil but containing 2% glucose. *dcp1Δdcp2Δ* strains expressing both GFP tagged Dcp2 mutants and Edc3-mCherry were grown in the same media also lacking lysine. Glucose starvation in Figure 1 – figure supplementary 4 and Figure 4 – figure supplement 1A was performed by exchanging with the corresponding synthetic medium lacking 2% glucose for durations indicated in the text. Stationary stage in Figure 4 – figure supplement 1B was achieved by growing cells for 5 days and OD_{600}

> 6. For imaging, cells were grown at 30 °C until OD_{600} = 0.4 ~ 0.6, and then immobilized on concanavalin-A (Sigma-Aldrich) coated glass bottom dishes (MatTek).

Image acquisition and analysis

All images were acquired using a Leica SP8 Laser Scanning Confocal Microscope using a 100 X 1.4 NA oil immersion objective. Images were analyzed using Fiji.

Identification of P bodies

For strains expressing only GFP tagged protein, P bodies were identified by thresholding the GFP fluorescence intensity using the MaxEntropy algorithm in Fiji. For strains expressing both GFP tagged proteins and Edc3-mCherry Figure 5 and Figure 6, Edc3-mCherry signals were thresholded (MaxEntropy) to identify P bodies, and created masks. Absolute concentrations of each Dcp2 mutants in P bodies and partition coefficients (P bodies within masks created by Edc3-mCherry signals) were analyzed as described below, using Edc3-mCherry signals to quantify size of P bodies. To determine fractions of cells having GFP puncta in Figure 5E, PC greater than 2 was chosen arbitrarily that punctate localization could be observed in GFP channel. Because the formation of and partitioning into biomolecular condensates are sensitive to protein expression levels, we eliminated cells with low expression (bottom 10% of the populations) and high expression (top 10% in the populations) of GFP and mCherry.

Measurements of absolute concentrations in P bodies and cytoplasm, and partition coefficients

To quantify the absolute concentrations of GFP-tagged proteins in P bodies, we assume that P bodies are spherical (based on the similar diameters in x and y when measured), and correct their measured intensities based on the point spread function (PSF) of our microscope (Fink et al., 1998). We determined the PSF using 0.2 um fluorescent microspheres (Invitrogen) imaged with the same optics, filters, zoom settings and pinhole settings used throughout our study. We then modeled (Matlab) the intensity-diluting effect of the PSF when imaging spheres of different sizes through convoluting the PSF with the sphere. This yielded a correction curve relating sphere diameter to the fraction of true

maximum intensity actually measured in the image (Figure 1 – figure supplement 2)(Fink et al., 1998), assuming all fluorescence intensity derived from the sphere and none derived from the surroundings. We limited our cellular analyses to P bodies with measured diameter > 0.33 um (most are 0.4 - 0.8 um in *dcp1Δ* strains), which is 1.1 times larger than the x-y PSF, and thus the size of P body can be accurately measured as the full width at half maximum intensity (FWHM) of the object. From the measured diameter in the x-y dimension, an assumption of spherical shape, and the correction curve, we determined the calibration factor (CF) for the P body intensity.

To determine P body intensity ($I_{Pbody,measured}$), we first measured the maximum intensity of P body and then drew a one pixel circle around it to find the surrounding pixels. 9 pixels including the maximal one were averaged to get the $I_{Pbody,measured}$. Since the correction was based on the assumption that all fluorescence intensity derived from the object, we applied it only to the incremental intensity of the P body over the cytoplasm ($I_{Pbody,measured}$-I_{cyto}); cytoplasmic intensity also contributes to $I_{Pbody,\ measured}$, but is homogenous across the cell and should not be corrected for the PSF effect. The real maximum intensity of P body(I_{Pbody}) was thus calculated as [($I_{Pbody,measured}$-I_{cyto})/CF + I_{cyto}]. Cytoplasm intensity was calculated by averaging the mean intensities of three ROIs the same size as P bodies in the cytoplasm.

We used standard curves of the fluorescence intensities of GFP solutions imaged with identical parameters as yeast to convert I_{Pbody} and I_{cyto} to absolute concentrations in P bodies (C_{Pbody}) and the cytoplasm (C_{cyto}). Because the intensities of P bodies marked by different proteins have a large dynamic range, to avoid saturation of our camera, we imaged them using different laser powers and gain settings, and generated different GFP standard curves accordingly. Partition coefficients were calculated as C_{Pbody}/C_{cyto}.

Total fractions in P bodies, average cellular concentration and number of molecules per cell

We collected z-stacks of yeast cells with a 0.22 um step size. To calculate the number of molecules in cytoplasm (N_{cyto}), we first measured the cell volume. Diameters in x, y and

z directions were measured manually with Otsu thresholding to determine the cell boundaries in Fiji. Cell volume was calculated as V_{cell} = 4/3*π*(x/2)*(y/x)*(z/2), assuming that yeast cells are ellipsoidal. Previous studies have shown that the cytoplasmic volume of a yeast cell is about 67% of the total cell volume (Uchida et al., 2011; Yamaguchi et al., 2011). To calculate the number of molecules in P bodies (N_{Pbody}), we measured the x-y diameter of each P body in the cell and calculated its volume by assuming a spherical shape. The concentrations in the cytoplasm (C_{cyto}) and P body (C_{Pbody}) were determined as described above. N_{cyto} and N_{Pbody} were calculated as $N_{cyto} = V_{cell} \times 0.67 \times C_{cyto} \times N_A$ (6.02×10^{23}). $N_{Pbody} = (\sum V_{Pbody} \times C_{Pbody}) \times N_A$ (6.02×10^{23}). Average cellular concentration = $((\sum V_{Pbody} \times C_{Pbody}) + V_{cell} \times 0.67 \times Ccyto)/ V_{cell} \times 0.67$. The fraction of molecules in P bodies is thus $N_{Pbody}/(N_{cyto} + N_{Pbody})$.

Fluorescence recovery after photobleaching (FRAP)

Selected P bodies were bleached using an 0.5 W 488 nm laser at 60% laser power. Images were collected from a single plane using a 2.5 airy unit pinhole at 5 s intervals for 150 s. Fluorescence intensities were analyzed manually in Fiji. Background intensities ($I_{background}$) were first subtracted. Because yeast cells are small, the cytoplasm may be bleached slightly while bleaching the P bodies. We thus measured the average fluorescence intensities of cytoplasm (excluding the bleached P body) before bleaching ($I_{cytobefore}$) and in the first frame after bleaching ($I_{cytoafter}$) to account for this effect. An unbleached P body was used to correct for the photo-bleaching during image acquisition in the recovery phase ($I_{unbleached}$). The corrected recovered intensities ($I_{recovery}$) were normalized to the intensities pre-bleaching ($I_{pre\text{-}bleaching}$).

$$I_{recovery} = \frac{(I - I_{background})}{(I_{unbleached} - I_{background})} \times \frac{(I_{cytoafter} - I_{background})}{(I_{cytobefore} - I_{background})}$$

$$I_t = \frac{I_{recovery}}{(I_{pre-bleaching} - I_{background})}$$

Normalized intensities were fitted to a single exponential recovery (one-phase association function in Prism) (GraphPad Software).

$$I_{(t)} = I_\infty + (I_0 - I_\infty)e^{-kt}$$

where I_0 , I_∞ and *k* were fit as intensity immediately after bleach, intensity at long times and the rate constant for recovery, respectively. The fractional recovery was calculated as:

$$F = \frac{I_\infty - I_0}{1 - I_0}$$

inverse FRAP (iFRAP)

For iFRAP, the whole cytoplasm except one P body was bleached 3 times for a total of 1.5 s using a 0.5 W 488 nm laser at 100% laser power. Fluorescence intensities were analyzed as in the FRAP experiments above. Because intensities of the unbleached P body were likely affected during bleaching, we normalized the intensity to the intensities of P body in the first frame after photo-bleaching (I_{pre}).

$$I_t = \frac{(I - I_{background})}{(I_{unbleached} - I_{background})} \times \frac{1}{(I_{pre} - I_{background})}$$

Normalized intensities were fitted to a single exponential decay (one-phase decay function in Prism) (GraphPad Software).

$$I_{(t)} = I_\infty + (I_0 - I_\infty)e^{-kt}$$

where I_0 , I_∞ and *k* were fitted parameters. The fractional decay was calculated as:

$$F = I_0 - I_\infty$$

Construction of connection map and calculation of centrality

Protein-protein and protein-RNA interactions were summarized from literatures as shown in Table 3. When counting number of interactions each protein makes to others, Lsm1-7 complex was treated as a whole entity, and all the other proteins were treated as individual molecules. The connection network was generated using Cytoscape (Shannon et al., 2003). Eigenvector centrality of each node was calculated using CytoNCA in Cytoscape (Tang et al., 2015), method in which connections to highly connected nodes contribute more to score of the questioned node than equal number of connections to less connected nodes. The size of nodes and the distance of other nodes to RNA node were manually adjusted to reflect eigenvector centrality.

Western blot

Yeast total extracts were prepared as previously described (Knop et al., 1999). 1.5 x 10^8 cells from OD_{600} = 0.4 – 0.6 cultures were resuspended in 1150 ul lysis buffer (0.24 M NaOH, 1% β-mercaptoethanol, 1 mM EDTA, 1 mM PMSF, 5 uM Pepstatin A, 10 uM Leupeptin). After incubation on ice for 20 min, 150 ul 55% trichloroacetic acid (TCA) was added to precipitate proteins on ice for 20 min. The mixture was centrifuged at 16100 rpm at 4 °C for 10 min. The pellet was resuspened in 250 ul HU buffer (8 M urea, 5% SDS, 200 mM Tris-HCl [pH 6.8], 1 mM EDTA, 5% β-mercaptoethanol, and 1% bromophenol blue) and incubated at 65 °C for 10 min, followed by 16100 rpm centrifugation at RT for 5 min. The supernatant was used for subsequent analyses. Immunoblotting was performed with primary antibodies: rabbit-anti-GFP (1:2000) (Abcam), and mouse-anti-PGK1 (1:1000) (Abcam). Mouse-anti-rabbit-IgG (1:10,000) (Santa Cruz) and goat-anti-mouse-IgG (1:10,000) (Santa Cruz) were used as secondary antibodies.

Quantifications and Statistical Analysis

Detailed statistics including number of cells analyzed, mean value, standard deviation and standard error of the mean are indicated in each figure legend. The Wilcoxon rank-sum test was performed using GraphPad Prism (GraphPad software). The Fligner-Killeen test was performed using R. Significance was determined as: ***, $p < 0.001$; ****, $p < 0.0005$.

Acknowledgements

We thank Saumya Jain for discussions on performing FRAP; Salman Banani, Jon Ditlev and Allyson Rice for helpful discussions on image analysis; Simon Currie and Jon Ditlev for critical reading of the manuscript; and members of the Rosen lab for helpful discussions. This work was supported by the Howard Hughes Medical Institute (M.K.R. and R.P.) and Welch Foundation (grant I-1544, M.K.R.).

Competing interests

Figure 1. Seven proteins are highly concentrated in P bodies

(A) Partition coefficients (PCs) of 19 P body proteins. Plots show PCs and mean values (blue line) ± standard error of the mean (SEM).
(B) Absolute concentrations in P bodies of 19 P body proteins. Plots show absolute concentrations in P bodies and mean values (red line) ± SEM.
For (A) and (B) each dot represents an individual P body. Red, core P body proteins. Black, non-core P body proteins. One P body per cell was analyzed from 16 - 25 cells for each protein.

Figure 1 – figure supplement 1. Punctate localization of GFP tagged proteins and co-localization with P body marker.
(A) Confocal fluorescence microscopy images of 31 P body proteins fused to GFP expressed in *dcp1Δ* strain in log-phase. Scale bar, 5 um.
(B) Fluorescence microscopy images of yeast co-expressing Edc3-mcherry and selected GFP-fused P body proteins. Scale bar, 5 um.

Figure 1 – figure supplement 2. Quantifications of protein concentrations using fluorescence intensities.
(A) Measure maximum intensity of P body and average intensity of cytoplasm.
(B) Measure size of P body by drawing a line across the P body and measure the full width at half maximum intensity (FWHM).
(C) The correction curve relates size of P body to the fraction of true maximum intensity measured in the image as indicated by the red line.
(D) Three standard curves generated by different concentrations of GFP solutions correspond to three different imaging settings.
(E) Partition coefficient is the ratio of P body concentration to cytoplasm concentration.

Figure 1 – figure supplement 3. Verification of quantitative measurements.
(A) A C-terminal GFP tag does not affect protein partitioning into P bodies. Plots show PC values (black dots) and means (red line)± SEM when Edc3 and Dhh1 tagged at their C-termini with either GFP or mCherry. Each dot represents an individual P body in one

cell. 18 - 20 cells were analyzed. Significance was calculated using the Wilcoxon rank-sum test.

(B) A C-terminal GFP tag does not affect protein dynamics. Recovery curve of C-terminal GFP- or mCherry-tagged Edc3 and Dhh1 as an average of 20 P bodies ± SD.

(C) Location of the GFP tag does not affect partitioning or dynamics of Dcp2. Dcp2 was tagged with GFP at either its N- (N-GFP-Dcp2) or C-terminus (Dcp2-GFP). Top: PCs (black dots) and mean value (red line)± SEM. Significance was calculated by Wilcoxon rank-sum test. Bottom: recovery curve as an average of 20 P bodies ± SD.

(D) Comparison of protein abundance (molecules per cell) measured in this study to previous unified database (Ho et al., 2018).

Figure 1 – figure supplement 4. Partitioning and dynamics of P body proteins in wild type strains under glucose starvation are qualitatively similar to *dcp1Δ* strains.

(A/B) Partition coefficients (A) or absolute concentrations (B) in P bodies in wild type strains under 30-60 min glucose starvation. Plots show PC values, and absolute concentrations in P bodies (black dots) and mean values (red line)± SEM. Each dot represents an individual P body in one cell. We analyzed 20 - 30 cells for each protein. Left, proteins found in both wild type and *dcp1Δ* strains ordered by their PC in *dcp1Δ* strains. Right, proteins only found in P bodies in wild type strains.

(C/D) Exchange rate (C) or fractional recovery (D) was plotted as a function of absolute concentrations in P bodies (mean± SEM). P body core and non-core proteins are indicated by red and black symbols, respectively.

Figure 2. Core proteins tend to have slow dynamics

Exchange rate (A) or fractional recovery (B) was plotted as a function of absolute concentrations in P bodies, respectively (mean ± SEM). Core and non-core proteins are indicated by red and black symbols, respectively. Graphs on the right show averaged exchange rate or fractional recovery (red lines) in core and non-core groups. Analysis of significance was calculated by Wilcoxon rank-sum test. *** and **** indicate p values less than 0.001 and 0.0005, respectively.

Figure 2 – figure supplement 1. FRAP recovery curves of 19 P body proteins.
FRAP recovery curves of 19 P body proteins reported as average of 16 - 25 P bodies ± SD.

Figure 2 – figure supplement 2. Slow dynamics are not caused by smaller fluorescence pool in cytoplasm.
(A/B) Exchange rate (A) or fractional recovery (B) is not correlated with protein concentrations in cytoplasm. Exchange rate or fractional recovery (mean± SEM) were plotted as a function of absolute concentrations in cytoplasm (mean± SEM), respectively. P body core and non-core proteins are indicated by red and black symbols, respectively.
(C/D) Exchange rate (C) or fractional decay (D) measured by iFRAP (16-20 cells measured for each protein) are qualitatively similar to values measured using FRAP. The fractional decay of more rapidly exchanging proteins measured by iFRAP is systematically smaller than measured using FRAP due to the longer time to bleach the whole cytoplasm in the former experiments. P body core and non-core proteins are indicated by red and black symbols, respectively. Pearson correlation coefficients were calculated in Prism (GraphPad).

Figure 2 – figure supplement 3. Protein-protein and protein-RNA connections among regular P body proteins.
Protein-protein and protein-RNA interactions are summarized from literatures as shown in Table 3. Red, core P body proteins. Black, non-core P body proteins. Grey, 12 P body proteins that lacked clear punctate localization in our studies. Size of node and distance of other nodes to RNA node reflect its centrality.

Figure 3. Partitioning of proteins into P bodies are correlated
(A) Schematics of calculations of ratios of paired and randomized proteins. Paired ones are ratios of X-GFP to Dcp2-mCherry in the same P bodies where i = i'. Randomized

pairing are achieved by randomly generating i and j in Excel where i ≠ j. The sample size are kept the same as paired ones.

(B/C/D) Concentrations of Edc3 and Dcp2 (A), Pat1 and Dcp2 (B), and Xrn1 and Dcp2 (C) are correlated in P bodies. Each dot represents one P body in a cell, 86 cells (B), 64 cells (C), and 135 cells (D) were analyzed. Pearson correlation coefficients were calculated in Prism (GraphPad softerware).

(E) Ratios of paired proteins have tighter ranges than ratios when randomizing pairing. Plots show ratios (black dots) and mean values ± standard deviation (red line, values are shown. Fligner-Killeen test was used to test equality of variance in R. ***, $p < 0.001$, ****, $p < 0.0005$.

Figure 4. P bodies do not strongly sequester their resident proteins

Plots show fractions in visible P bodies (black dots) and mean values (red lines) ± SEM in mid-log phase without any cellular stress. Each dot represents fraction of protein in visible P bodies corresponding to an individual cell. 16 - 25 cells were analyzed for each protein.

Figure 4 – figure supplement 1. P bodies do not strongly sequester their resident proteins.

(A) Fractions of total protein localized to P bodies (black dots) and mean values (red lines) ± SEM in *dcp1Δ* strains. Cells were grown to mid-log phase followed by 4h glucose starvation.

(B) Fractions of total protein localized to P bodies (black dots) and mean values (red lines) ± SEM in *dcp1Δ* strains in stationary phase. In A and B, each dot corresponds to an individual cell, and 20 cells were analyzed for each protein.

Figure 5. Elements controlling Dcp2 partitioning and dynamics are distributed across the protein, and contribute to specific recruitment to biomolecular condensates.

(A) Schematics of domain architecture of Dcp2 FL and mutants. Red, N-terminal domain (NTD). Orange, HLM1. Blue, other 10 HLMs in C-terminal domain. Grey, inactivated

HLMs.

(B/C) Partition coefficients (B) and dynamics (C) of GFP tagged Dcp2 FL (black), Dcp2ΔN (red), Dcp2 ΔH1 (orange), and Dcp2 300 (grey) in *dcp1Δdcp2Δ* strain. One P body per cell was analyzed from 19 cells. PCs are shown as mean values (bold horizontal bars) ± SEM (B). Recovery curves are shown as average of 19 P bodies ± SEM (C). Significance was calculated by the Wilcoxon rank-sum test. *** and **** indicate p values less than 0.001 and 0.0005, respectively.

(D) Representative images showing *dcp1Δdcp2Δ* yeast strains expressing GFP tagged Dcp2 300 ΔH1, Dcp2C Δ5H and Dcp2 ΔH1 Δ5H. Edc3-mCherry was also expressed as a P body marker. Scale bar, 5 um.

(E) Fractions of cells exhibiting puncta formed by each mutant. n(Dcp2 300 ΔH1) = 163, n(Dcp2C Δ5H) = 188, n(Dcp2 ΔH1 Δ5H) = 204.

(F) Partition coefficients of GFP-tagged Dcp2 300 ΔH1, Dcp2C Δ5H and Dcp2 ΔH1 Δ5H, and mean values (red bold horizontal bars) ± SEM. 100 P bodies were analyzed. Significance was calculated by the Wilcoxon rank-sum test. **** indicates p values less than 0.0005.

(G) Specific recruitment to P bodies can be achieved by distributing elements across Dcp2.

Figure 5 – figure supplement 1.

(A) Representative images of *dcp1Δdcp2Δ* yeas*t* expressing Edc3-mCherry as a P body marker. Scale bar, 5 um.

(B) Western blot of Dcp2 FL, Dcp2 300, and Dcp2 ΔN in *dcp1Δdcp2Δ* strain shows that they expressed at similar levels.

(C) Western blot of Dcp2 300 ΔH1, Dcp2C Δ5H and Dcp2 ΔH1 Δ5H in *dcp1Δdcp2Δ* strain shows that they expressed at similar levels.

Figure 6. Partitioning of Dcp2 into P bodies can be saturated

(A) Schematics of domain architecture of Dcp2 FL, Dcp2 FL-H1, Dcp2CΔ5H, and Dcp2CΔ5H-H1.

(B) Representative images showing *dcp1Δdcp2Δ* yeast strains expressing GFP tagged Dcp2 FL, Dcp2 FL-H1, Dcp2CΔ5H, and Dcp2CΔ5H-H1, with Edc3-mCherry co-expressed as a P body marker. Scale bar, 5 um.

(C/D) P body concentrations/PCs of Dcp2 FL (n=49), Dcp2 FL-H1 (n=79), Dcp2CΔ5H (n=63), and Dcp2CΔ5H-H1 (n=52), and mean values (bold horizontal bars) ± SEM.

Figure 6 – figure supplement 1

Average cellular concentrations of Dcp2 FL, Dcp2 FL-H1, Dcp2CΔ5H, and Dcp2CΔ5H-H1 in *dcp1Δdcp2Δ* strain expressing Edc3-mCherry, and mean values (red horizontal bars) ± SEM.

Figure 7. RNA binding and turnover affect Dcp2 partitioning and dynamics

(A) Schematics of domain architecture of Dcp2 300, Dcp2 300 AAAA, Dcp2 ΔH1 and Dcp2 ΔH1 WD.

(B) Representative images of dcp1*Δdcp2Δ* yeast strain expressing GFP tagged Dcp2 300 and Dcp2 300 AAAA. Scale bar, 5 um.

(C) Representative images of *dcp2Δ* yeast strain expressing GFP tagged Dcp2 ΔH1 and Dcp2 ΔH1 WD under normal and glucose starvation conditions. Scale bar, 5 um.

(D) Inhibition of RNA turnover promotes P body formation. Number of P bodies formed by Dcp2 ΔH1 (blue, n=115) and Dcp2 ΔH1 WD (red, n=91) under normal conditions, Dcp2 ΔH1 (light blue, n=119) and Dcp2 ΔH1 WD (light red, n=144) under 30-60min glucose starvation.

(E) Inhibition of RNA turnover promotes more Dcp2 ΔH1 to partition into P bodies. Total fractions of Dcp2 ΔH1(blue, n=20) and Dcp2 ΔH1 WD (red, n=20) without stress, and Dcp2 ΔH1(light blue, n=23) and Dcp2 ΔH1 WD (light red, n=32) with glucose starvation, in P bodies. Numbers show mean values ± SEM. Significance was calculated by the Wilcoxon rank-sum test. ****, $p < 0.0005$

(F) Inhibition of RNA turnover slows Dcp2 ΔH1 exchange rate by increasing amount of RNA. Top, FRAP recovery curves of Dcp2 ΔH1 (blue, n=20) and Dcp2 ΔH1 WD (red,

n=20) without stress. Bottom, FRAP recovery curves of Dcp2 ΔH1 (light blue, n=23) and Dcp2 ΔH1 WD (light red, n=32) under glucose starvation.

Figure 7 – figure supplement 1

(A) Western blot of Dcp2 300 and Dcp2 300 AAAA in *dcp1Δ dcp2Δ* strain shows that they expressed at similar levels.

(B) Western blot of Dcp2 ΔH1 and Dcp2 ΔH1 WD in *dcp2Δ* strain shows that they expressed at similar levels.

References

Alberti, S., and Dormann, D. (2019). Liquid-liquid phase separation in disease. Annu Rev Genet 53, 171-194.

Aizer, A., Kalo, A., Kafri, P., Shraga, A., Ben-Yishay, R., Jacob, A., Kinor, N., and Shav-Tal, Y. (2014). Quantifying mRNA targeting to P bodies in living human cells reveals their dual role in mRNA decay and storage. J Cell Sci *127*, 4443-4456.

Anderson, J.S., Lyon, C.E., Fox, A.H., Leung, A.K.L., Lam, Y. W., Steen, H., Mann, M., Lamond, A. (2002). Directed Proteomic Analysis of the Human Nucleolus. Curr Biol *12*, 1-11.

Arimoto, K., Fukuda, H., Imajoh-Ohmi, S., Saito, H., and Takekawa, M. (2008). Formation of stress granules inhibits apoptosis by suppressing stress-responsive MAPK pathways. Nat Cell Biol *10*, 1324-1332.

Banani, S.F., Rice, A.M., Peeples, W.B., Lin, Y., Jain, S., Parker, R., and Rosen, M.K. (2016). Compositional Control of Phase-Separated Cellular Bodies. Cell *166*, 651-663.

Banani, S.F., Lee, H.O., Hyman, A.A., and Rosen, M.K. (2017). Biomolecular condensates: organizers of cellular biochemistry. Nat Rev Mol Cell Biol *18*, 285-298.

Basquin, J., Roudko, V.V., Rode, M., Basquin, C., Seraphin, B., and Conti, E. (2012). Architecture of the nuclease module of the yeast Ccr4-not complex: the Not1-Caf1-Ccr4 interaction. Mol Cell *48*, 207-218.

Beutel, O., Maraspini, R., Pombo-Garcia, K., Martin-Lemaitre, C., and Honigmann, A. (2019). Phase Separation of Zonula Occludens Proteins Drives Formation of Tight Junctions. Cell *179*, 923-936 e911.

Bhattacharyya, S.N., Habermacher, R., Martine, U., Closs, E.I., and Filipowicz, W. (2006). Relief of microRNA-mediated translational repression in human cells subjected to stress. Cell *125*, 1111-1124.

Bhaskar, V., Roudko, V., Basquin, J., Sharma, K., Urlaub, H., Seraphin, B., and Conti, E. (2013). Structure and RNA-binding properties of the Not1-Not2-Not5 module of the yeast Ccr4-Not complex. Nat Struct Mol Biol *20*, 1281-1288.

Blewett, N.H., and Goldstrohm, A.C. (2012). A eukaryotic translation initiation factor 4E-binding protein promotes mRNA decapping and is required for PUF repression. Mol Cell Biol *32*, 4181-4194.

Brangwynne, C.P., Eckmann, C.R.M, Courson, D.S., Rybarska, A., Hoege, C., Gharakhani, J., Jülicher, F., Hyman, A.A. (2009). Germline P Granules Are Liquid Droplets That Localize by Controlled Dissolution/Condensation. Science *324*, 1729-1732.

Brangwynne, C.P., Mitchison, T.J., and Hyman, A.A. (2011). Active liquid-like behavior of nucleoli determines their size and shape in Xenopus laevis oocytes. Proc Natl Acad Sci U S A *108*, 4334-4339.

Buchan, J.R., Muhlrad, D., and Parker, R. (2008). P bodies promote stress granule assembly in *Saccharomyces cerevisiae*. J Cell Biol, *183*, 441–455.

Charenton, C., Taverniti, V., Gaudon-Plesse, C., Back, R., Seraphin, B., and Graille, M. (2016). Structure of the active form of Dcp1-Dcp2 decapping enzyme bound to m(7)GDP and its Edc3 activator. Nat Struct Mol Biol *23*, 982-986.

Coller, J. M., Tucker, M., Sheth, U., Valencia-Sanchez, M. A., & Parker, R. (2001). The DEAD box helicase, Dhh1p, functions in mRNA decapping and interacts with both the decapping and deadenylase complexes. RNA *7*, 1717–1727.

Cougot, N., Babajko, S., and Seraphin, B. (2004). Cytoplasmic foci are sites of mRNA decay in human cells. J Cell Biol *165*, 31-40.

Decker, C.J., Teixeira, D., and Parker, R. (2007). Edc3p and a glutamine/asparagine-rich domain of Lsm4p function in processing body assembly in Saccharomyces cerevisiae. J Cell Biol *179*, 437-449.

Decker, C.J., and Parker, R. (2012). P bodies and stress granules: possible roles in the control of translation and mRNA degradation. Cold Spring Harb Perspect Biol *4*, a012286.

Deshmukh, M.V., Jones, B.N., Quang-Dang, D.U., Flinders, J., Floor, S.N., Kim, C., Jemielity, J., Kalek, M., Darzynkiewicz, E., and Gross, J.D. (2008). mRNA decapping is promoted by an RNA-binding channel in Dcp2. Mol Cell *29*, 324-336.

Ditlev, J.A., Case, L.B., and Rosen, M.K. (2018). Who's in and Who's Out-Compositional Control of Biomolecular Condensates. J Mol Biol.

Dunckley, T., Tucker, M., and Parker, R. (2001). Two related proteins, Edc1p and Edc2p, stimulate mRNA decapping in Saccharomyces cerevisiae. Genetics *157*, 27–37.

Dundr, M., Hebert, M.D., Karpova, T.S., Stanek, D., Xu, H., Shpargel, K.B., Meier, U.T., Neugebauer, K.M., Matera, A.G., and Misteli, T. (2004). In vivo kinetics of Cajal body components. J Cell Biol *164*, 831-842.

Falahati, H., and Wieschaus, E. (2017). Independent active and thermodynamic processes govern the nucleolus assembly in vivo. Proc Natl Acad Sci U S A *114*, 1335-1340.

Fernandes, N., and Buchan, J.B. (2019). *RPS28B* mRNA acts as a scaffold promoting *cis*-translational interaction of proteins driving P-body assembly. bioRxiv.

Fink, C., Morgan, F., Loew, L.M. (1998). Intracellular Fluorescent Probe Concentrations by Confocal Microscopy. Biophys J *75*, 1648-1658.

Floor, S.N., Jones, B.N., Hernandez, G.A., and Gross, J.D. (2010). A split active site couples cap recognition by Dcp2 to activation. Nat Struct Mol Biol *17*, 1096-1101.

Fromm, S.A., Kamenz, J., Noldeke, E.R., Neu, A., Zocher, G., and Sprangers, R. (2014). In vitro reconstitution of a cellular phase-transition process that involves the mRNA decapping machinery. Angew Chem Int Ed Engl *53*, 7354-7359.

Georgiev, A., Sjostrom, M., and Wieslander, A. (2007). Binding specificities of the GYF domains from two Saccharomyces cerevisiae paralogs. Protein Eng Des Sel *20*, 443-452.

Gibson, B.A., Doolittle, L.K., Schneider, M.W.G., Jensen, L.E., Gamarra, N., Henry, L., Gerlich, D.W., Redding, S., and Rosen, M.K. (2019). Organization of Chromatin by Intrinsic and Regulated Phase Separation. Cell *179*, 470-484 e421.

Gietz, R.D., and Schiestl, R.H. (2007). High-efficiency yeast transformation using the LiAc/SS carrier DNA/PEG method. Nat Protoc *2*, 31-34.

Harigaya, Y., Jones, B.N., Muhlrad, D., Gross, J.D., and Parker, R. (2010). Identification and analysis of the interaction between Edc3 and Dcp2 in Saccharomyces cerevisiae. Mol Cell Biol *30*, 1446-1456.

He, F., Brown, A. H., & Jacobson, A. (1997). Upf1p, Nmd2p, and Upf3p are interacting components of the yeast nonsense-mediated mRNA decay pathway. Mol Cell Biol *17*, 1580–1594.

Ho, B., Baryshnikova, A., and Brown, G.W. (2018). Unification of Protein Abundance Datasets Yields a Quantitative Saccharomyces cerevisiae Proteome. Cell Syst *6*, 192-205 e193.

Hondele, M., Sachdev, R., Heinrich, S., Wang, J., Vallotton, P., Fontoura, B.M.A., and Weis, K. (2019). DEAD-box ATPases are global regulators of phase-separated organelles. Nature *573*, 144-148.

Hubstenberger, A., Courel, M., Benard, M., Souquere, S., Ernoult-Lange, M., Chouaib, R., Yi, Z., Morlot, J.B., Munier, A., Fradet, M.*, et al.* (2017). P body Purification Reveals the Condensation of Repressed mRNA Regulons. Mol Cell *68*, 144-157 e145.

Ingelfinger, D., Arndt-Jovin, D.J., Lührmann, R., Achsel, T. (2002). The human LSm1-7 proteins colocalize with the mRNA-degrading enzymes Dcp1/2 and Xrn1 in distinct cytoplasmic foci. RNA *8*, 1489-1501.

Irie, K., Tadauchi, T., Takizawa, P. A., Vale, R. D., Matsumoto, K., and Herskowitz, I. (2002). The Khd1 protein, which has three KH RNA-binding motifs, is required for proper localization of *ASH1* mRNA in yeast. EMBO J *21*, 1158–1167.

Jain, S., Wheeler, J.R., Walters, R.W., Agrawal, A., Barsic, A., and Parker, R. (2016). ATPase-Modulated Stress Granules Contain a Diverse Proteome and Substructure. Cell *164*, 487-498.

Kato, M., Han, T.W., Xie, S., Shi, K., Du, X., Wu, L.C., Mirzaei, H., Goldsmith, E.J., Longgood, J., Pei, J.*, et al.* (2012). Cell-free formation of RNA granules: low complexity sequence domains form dynamic fibers within hydrogels. Cell *149*, 753-767.

Khong, A., Matheny, T., Jain, S., Mitchell, S.F., Wheeler, J.R., and Parker, R. (2017). The Stress Granule Transcriptome Reveals Principles of mRNA Accumulation in Stress Granules. Mol Cell *68*, 808-820 e805.

Knop, M., Siegers, K., Pereira, G., Zachariae, W., Winsor, B., Nasmyth, K., and Schiebel, E. (1999). Epitope tagging of yeast genes using a PCR-based strategy: more tags and improved practical routines. Yeast *15*, 963–972.

Krogan, N.J., Cagney, G., Yu, H., Zhong, G., Guo, X., Ignatchenko, A., Li, J., Pu, S., Datta, N., Tikuisis, A.P.*, et al.* (2006). Global landscape of protein complexes in the yeast Saccharomyces cerevisiae. Nature *440*, 637-643.

Kshirsagar, M., and Parker, R. (2004). Identification of Edc3p as an enhance of mRNA decapping in Saccharomyces verevisiae. Genetics *166*, 729-739.

Kurischko, C., Kim, H.K., Kuravi, V.K., Pratzka, J., and Luca, F.C. (2011). The yeast Cbk1 kinase regulates mRNA localization via the mRNA-binding protein Ssd1. J Cell Biol *192*, 583-598.

Lallemand-Breitenbach, V., and de The, H. (2010). PML nuclear bodies. Cold Spring Harb Perspect Biol *2*, a000661.

Larson, A.G., Elnatan, D., Keenen, M.M., Trnka, M.J., Johnston, J.B., Burlingame, A.L., Agard, D.A., Redding, S., and Narlikar, G.J. (2017). Liquid droplet formation by HP1alpha suggests a role for phase separation in heterochromatin. Nature *547*, 236-240.

Leung, A.K., Calabrese, J.M., Sharp, P.A. (2006) Quantitative analysis of Argonaute protein reveals microRNA-dependent localization to stress granules. Pro. Natl. Acad. Sci. USA *103*, 18125-18130.

Li, H., Leo, C., Zhu, J., Wu, X., O'Neil, J., Park, E., Chen, J. D. (2000). Sequestration and Inhibition of Daxx-Mediated Transcriptional Repression by PML. Mol Cell Biol *20*, 1784-1796.

Li, K., Zhao, K., Ossareh-Nazari, B., Da, G., Dargemont, C., and Marmorstein, R. (2005). Structural basis for interaction between the Ubp3 deubiquitinating enzyme and its Bre5 cofactor. J Biol Chem *280*, 29176-29185.

Li, P., Banjade, S., Cheng, H.C., Kim, S., Chen, B., Guo, L., Llaguno, M., Hollingsworth, J.V., King, D.S., Banani, S.F.*, et al.* (2012). Phase transitions in the assembly of multivalent signalling proteins. Nature *483*, 336-340.

Lin, Y., Protter, D.S., Rosen, M.K., and Parker, R. (2015). Formation and Maturation of Phase-Separated Liquid Droplets by RNA-Binding Proteins. Mol Cell *60*, 208-219.

Ling, S.H., Decker, C.J., Walsh, M.A., She, M., Parker, R., Song, H. (2008). Crystal structure of human Edc3 and its functional implications. Mol Cell Biol *28*, 5965-76.

Lotan, R., Bar-On, V.G., Harel-Sharvit, L., Duek, L., Melamed, D., and Choder, M. (2005). The RNA polymerase II subunit Rpb4p mediates decay of a specific class of mRNAs. Genes Dev *19*, 3004–3016.

Lotan, R., Goler-Baron, V., Duek, L., Haimovich, G., and Choder, M. (2007). The Rpb7p subunit of yeast RNA polymerase II plays roles in the two major cytoplasmic mRNA decay mechanisms. J Cell Biol *178*, 1133-1143.

Malys, N., and McCarthy, J.E. (2006). Dcs2, a novel stress-induced modulator of m7GpppX pyrophosphatase activity that locates to P bodies. J Mol Biol *363*, 370-382.

Markmiller, S., Soltanieh, S., Server, K.L., Mak, R., Jin, W., Fang, M.Y., Luo, E.C., Krach, F., Yang, D., Sen, A.*, et al.* (2018). Context-Dependent and Disease-Specific Diversity in Protein Interactions within Stress Granules. Cell *172*, 590-604 e513.

Mitchell, S.F., Jain, S., She, M., and Parker, R. (2013). Global analysis of yeast mRNPs. Nat Struct Mol Biol *20*, 127-133.

Mugler, C.F., Hondele, M., Heinrich, S., Sachdev, R., Vallotton, P., Koek, A.Y., Chan, L.Y., and Weis, K. (2016). ATPase activity of the DEAD-box protein Dhh1 controls processing body formation. Elife *5*.

Neef, D.W., and Thiele, D.J. (2009). Enhancer of decapping proteins 1 and 2 are important for translation during heat stress in *Saccharomyces cerevisiae*. Mol Microbiol, *73*, 1032–1042.

Nissan, T., Rajyaguru, P., She, M., Song, H., and Parker, R. (2010). Decapping activators in Saccharomyces cerevisiae act by multiple mechanisms. Mol Cell *39*, 773-783.

Nott, T.J., Petsalaki, E., Farber, P., Jervis, D., Fussner, E., Plochowietz, A., Craggs, T.D., Bazett-Jones, D.P., Pawson, T., Forman-Kay, J.D.*, et al.* (2015). Phase transition of a disordered nuage protein generates environmentally responsive membraneless organelles. Mol Cell *57*, 936-947.

Pilkington, G.R., and Parker, R. (2008). Pat1 contains distinct functional domains that promote P body assembly and activation of decapping. Mol Cell Biol *28*, 1298-1312.

Protter, D.S.W., Rao, B.S., Van Treeck, B., Lin, Y., Mizoue, L., Rosen, M.K., and Parker, R. (2018). Intrinsically Disordered Regions Can Contribute Promiscuous Interactions to RNP Granule Assembly. Cell Rep *22*, 1401-1412.

Rajyaguru, P., She, M., and Parker, R. (2012). Scd6 targets eIF4G to repress translation: RGG motif proteins as a class of eIF4G-binding proteins. Mol Cell *45*, 244-254.

Rao, B.S., and Parker, R. (2017). Numerous interactions act redundantly to assemble a tunable size of P bodies in Saccharomyces cerevisiae. Proc Natl Acad Sci U S A *114*, E9569-E9578.

Riback, J.A., Katanski, C.D., Kear-Scott, J.L., Pilipenko, E.V., Rojek, A.E., Sosnick, T.R., and Drummond, D.A. (2017). Stress-Triggered Phase Separation Is an Adaptive, Evolutionarily Tuned Response. Cell *168*, 1028-1040 e1019.

Saha, S., Weber, C.A., Nousch, M., Adame-Arana, O., Hoege, C., Hein, M.Y., Osborne-Nishimura, E., Mahamid, J., Jahnel, M., Jawerth, L.*, et al.* (2016). Polar Positioning of

Phase-Separated Liquid Compartments in Cells Regulated by an mRNA Competition Mechanism. Cell *166*, 1572-1584 e1516.

Schütz, S., Noldeke, E.R., and Sprangers, R. (2017). A synergistic network of interactions promotes the formation of in vitro processing bodies and protects mRNA against decapping. Nucleic Acids Res *45*, 6911-6922.

Schwartz, D., Decker, C. J., and Parker, R. (2003). The enhancer of decapping proteins, Edc1p and Edc2p, bind RNA and stimulate the activity of the decapping enzyme. RNA *9*, 239–251.

Sharif, H., and Conti, E. (2013). Architecture of the Lsm1-7-Pat1 complex: a conserved assembly in eukaryotic mRNA turnover. Cell Rep *5*, 283-291.

Sheth, U., Parker, R. (2003). Decapping and Decay of Messenger RNA Occur in Cytoplasmic Processing Bodies. Science *300*, 805-808.

Sheth, U., and Parker, R. (2006). Targeting of aberrant mRNAs to cytoplasmic processing bodies. Cell *125*, 1095-1109.

Shin, Y., and Brangwynne, C.P. (2017). Liquid phase condensation in cell physiology and disease. Science *357*.

Simpson, C.E., Lui, J., Kershaw, C.J., Sims, P.F., and Ashe, M.P. (2014). mRNA localization to P bodies in yeast is bi-phasic with many mRNAs captured in a late Bfr1p-dependent wave. J Cell Sci *127*, 1254-1262.

Smith, J., Calidas, D., Schmidt, H., Lu, T., Rasoloson, D., and Seydoux, G. (2016). Spatial patterning of P granules by RNA-induced phase separation of the intrinsically-disordered protein MEG-3. Elife *5*.

Strom, A.R., Emelyanov, A.V., Mir, M., Fyodorov, D.V., Darzacq, X., and Karpen, G.H. (2017). Phase separation drives heterochromatin domain formation. Nature *547*, 241-245.

Su, X., Ditlev, J.A., Hui,E., Xing, W., Julia Okrut, J., King, D.S., Taunton, J., Rosen, M.K., Vale, R.D. (2016). Phase separation of signaling molecules promotes T cell receptor signal transduction. Science *352*, 595-599.

Sweet, T.J., Boyer, B., Hu, W., Baker, K.E., and Coller, J. (2007). Microtubule disruption stimulates P body formation. RNA *13*, 493-502.

Swisher, K.D., and Parker, R. (2011). Interactions between Upf1 and the decapping factors Edc3 and Pat1 in Saccharomyces cerevisiae. PLoS One *6*, e26547.

Tauber, D., Tauber, G., Khong, A., Van Treeck, B., Pelletier, J., and Parker, R. (2020). Modulation of RNA Condensation by the DEAD-Box Protein eIF4A. Cell *180*, 411-426 e416.

Teixeira, D., Sheth, U., Valencia-Sanchez, M.A., Brengues, M., and Parker, R. (2005). Processing bodies require RNA for assembly and contain nontranslating mRNAs. RNA *11*, 371-382.

Teixeira, D., Parker, R. (2007). Analysis of P body Assembly in Saccharomyces cerevisiae. Mol Biol Cell *18*, 2274-2287.

Uchida, M., Sun, Y., McDermott, G., Knoechel, C., Le Gros, M.A., Parkinson, D., Drubin, D.G., and Larabell, C.A. (2011). Quantitative analysis of yeast internal architecture using soft X-ray tomography. Yeast *28*, 227-236.

Uesono, Y., Toh-e, A., and Kikuchi, Y. (1997). Ssd1p of Saccharomyces cerevisiae Associates with RNA. J Biol Chem *272*, 16103-16109.

van Dijk, E., Cougot, N., Meyer, S., Babajko, S., Wahle, E., Séraphin, B. (2002). Human Dcp2: a catalytically active mRNA decapping enzyme located in specific cytoplasmic structures. EMBO J *21*, 6915-6924.

Wang, J.T., Smith, J., Chen, B.C., Schmidt, H., Rasoloson, D., Paix, A., Lambrus, B.G., Calidas, D., Betzig, E., and Seydoux, G. (2014). Regulation of RNA granule dynamics by phosphorylation of serine-rich, intrinsically disordered proteins in C. elegans. Elife *3*, e04591.

Weber, S.C., and Brangwynne, C.P. (2015). Inverse size scaling of the nucleolus by a concentration-dependent phase transition. Curr Biol *25*, 641-646.

Weidtkamp-Peters, S., Lenser, T., Negorev, D., Gerstner, N., Hofmann, T.G., Schwanitz, G., Hoischen, C., Maul, G., Dittrich, P., and Hemmerich, P. (2008). Dynamics of component exchange at PML nuclear bodies. J Cell Sci *121*, 2731-2743.

Wheeler, J.R., Jain, S., Khong, A., and Parker, R. (2017). Isolation of yeast and mammalian stress granule cores. Methods *126*, 12-17.

Woodruff, J.B., Ferreira Gomes, B., Widlund, P.O., Mahamid, J., Honigmann, A., and Hyman, A.A. (2017). The Centrosome Is a Selective Condensate that Nucleates Microtubules by Concentrating Tubulin. Cell *169*, 1066-1077 e1010.

Yamaguchi, M., Namiki, Y., Okada, H., Mori, Y., Furukawa, H., Wang, J., Ohkusu, M., and Kawamoto, S. (2011). Structome of Saccharomyces cerevisiae determined by freeze-substitution and serial ultrathin-sectioning electron microscopy. J Electron Microsc (Tokyo) *60*, 321-335.

Youn, J.Y., Dunham, W.H., Hong, S.J., Knight, J.D.R., Bashkurov, M., Chen, G.I., Bagci, H., Rathod, B., MacLeod, G., Eng, S.W.M.*, et al.* (2018). High-Density Proximity Mapping Reveals the Subcellular Organization of mRNA-Associated Granules and Bodies. Mol Cell *69*, 517-532 e511.

Figure 1

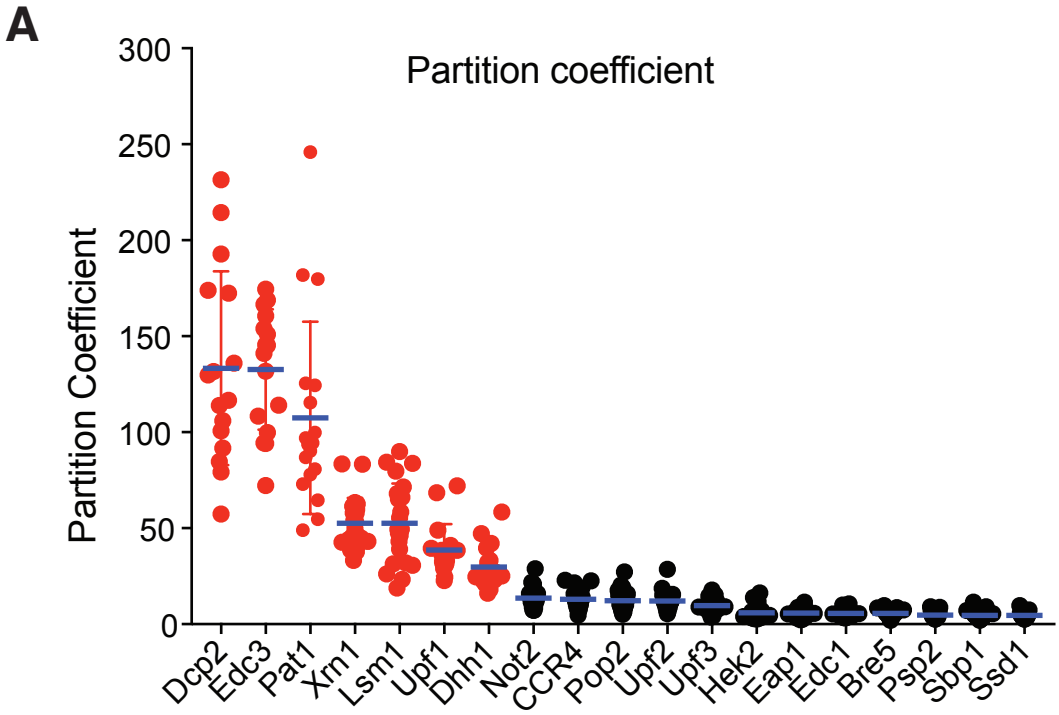
A
Partition coefficient
Partition Coefficient
300
250
200
150
100
50
0
Dcp2
Edc3
Pat1
Xrn1
Lsm1
Upf1
Dhh1
Not2
CCR4
Pop2
Upf2
Upf3
Hek2
Eap1
Edc1
Bre5
Psp2
Sbp1
Ssd1

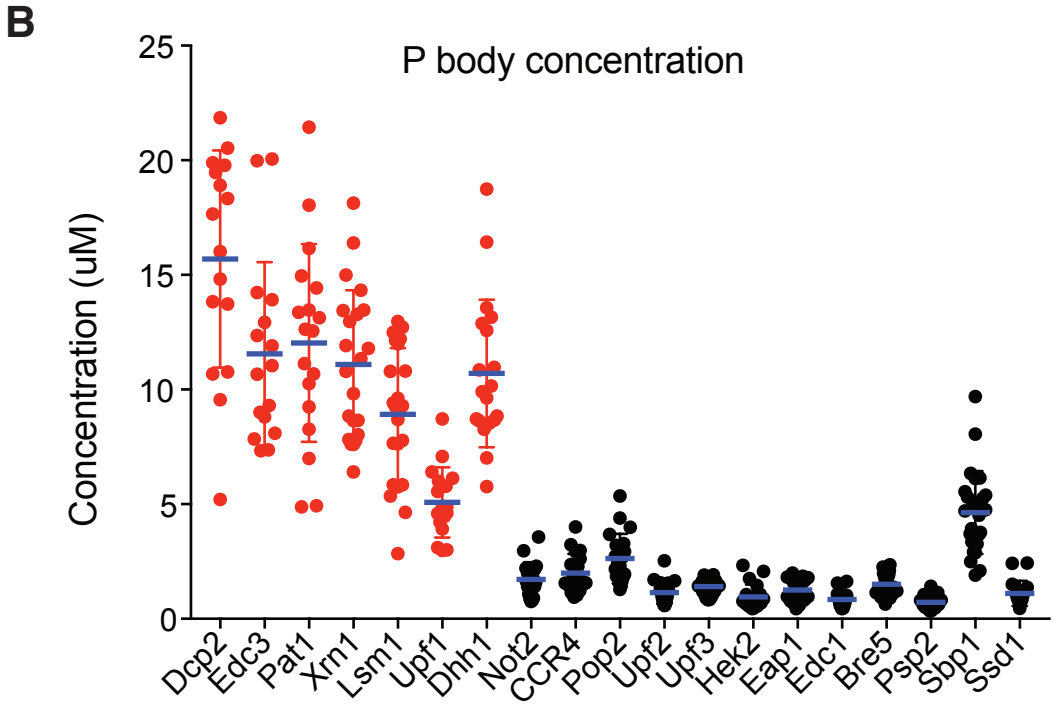
B
P body concentration
Concentration (uM)
25
20
15
10
5
0
Dcp2
Edc3
Pat1
Xrn1
Lsm1
Upf1
Dhh1
Not2
CCR4
Pop2
Upf2
Upf3
Hek2
Eap1
Edc1
Bre5
Psp2
Sbp1
Ssd1

Figure 1 - figure supplement 1

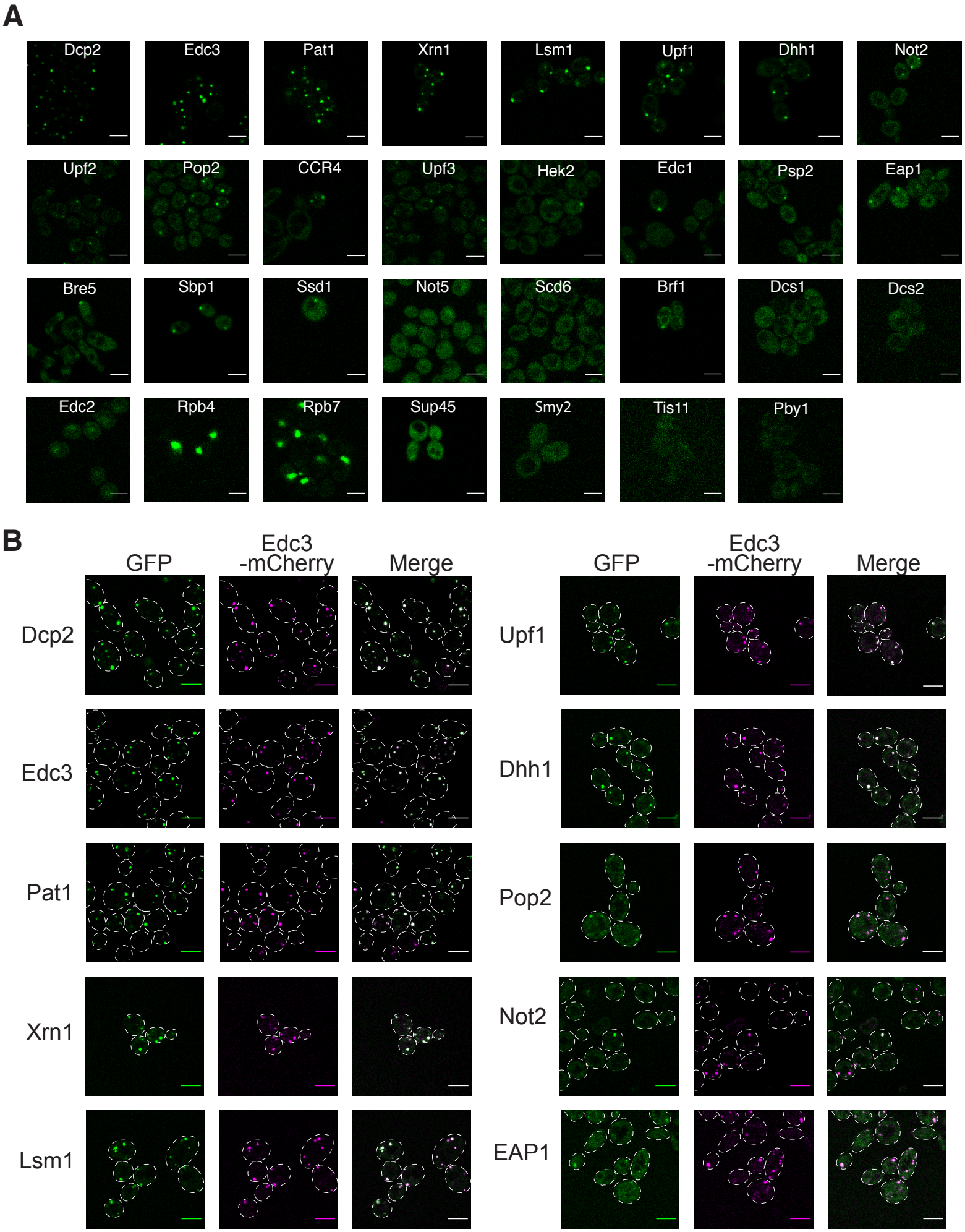

Figure 1 - figure supplement 2

A Measure P body intensity and cytoplasm intensity

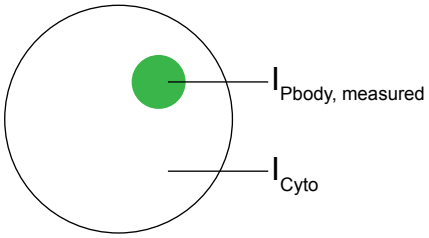

B Measure P body size as FWHM

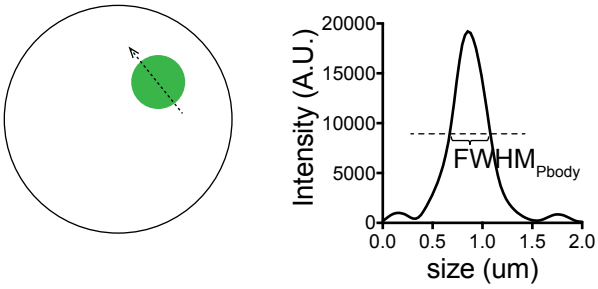

C Calculate correction factor and real P body intensity

$$\text{object size} = \frac{FWHM_{Pbody}}{PSF(xy)}$$

$$I_{Pbody} = \frac{I_{Pbody,\ measured} - I_{cyto}}{CF} + I_{cyto}$$

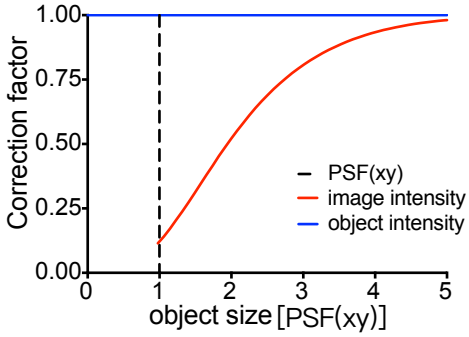

D Convert intensity to concentration using GFP standard curves.

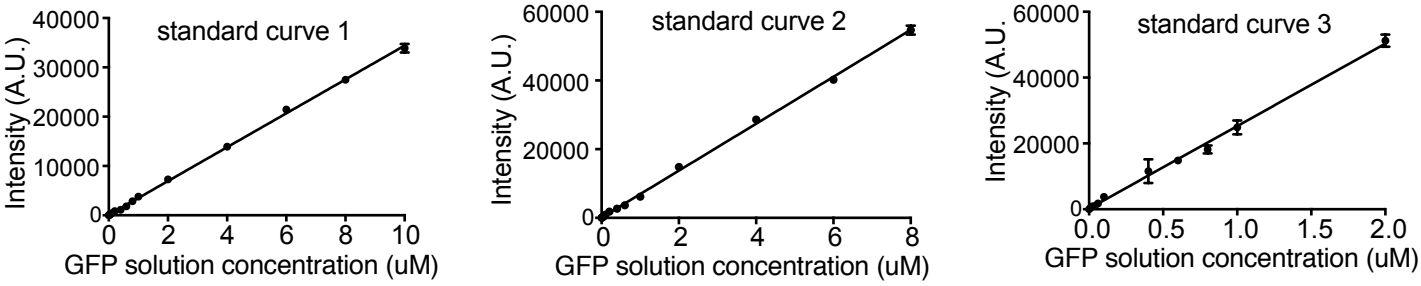

E Calculate Partition coefficient

$$\text{Partition coefficient} = \frac{Concentration_{Pbody}}{Concentration_{cyto}}$$

Figure 1 - figure supplement 3

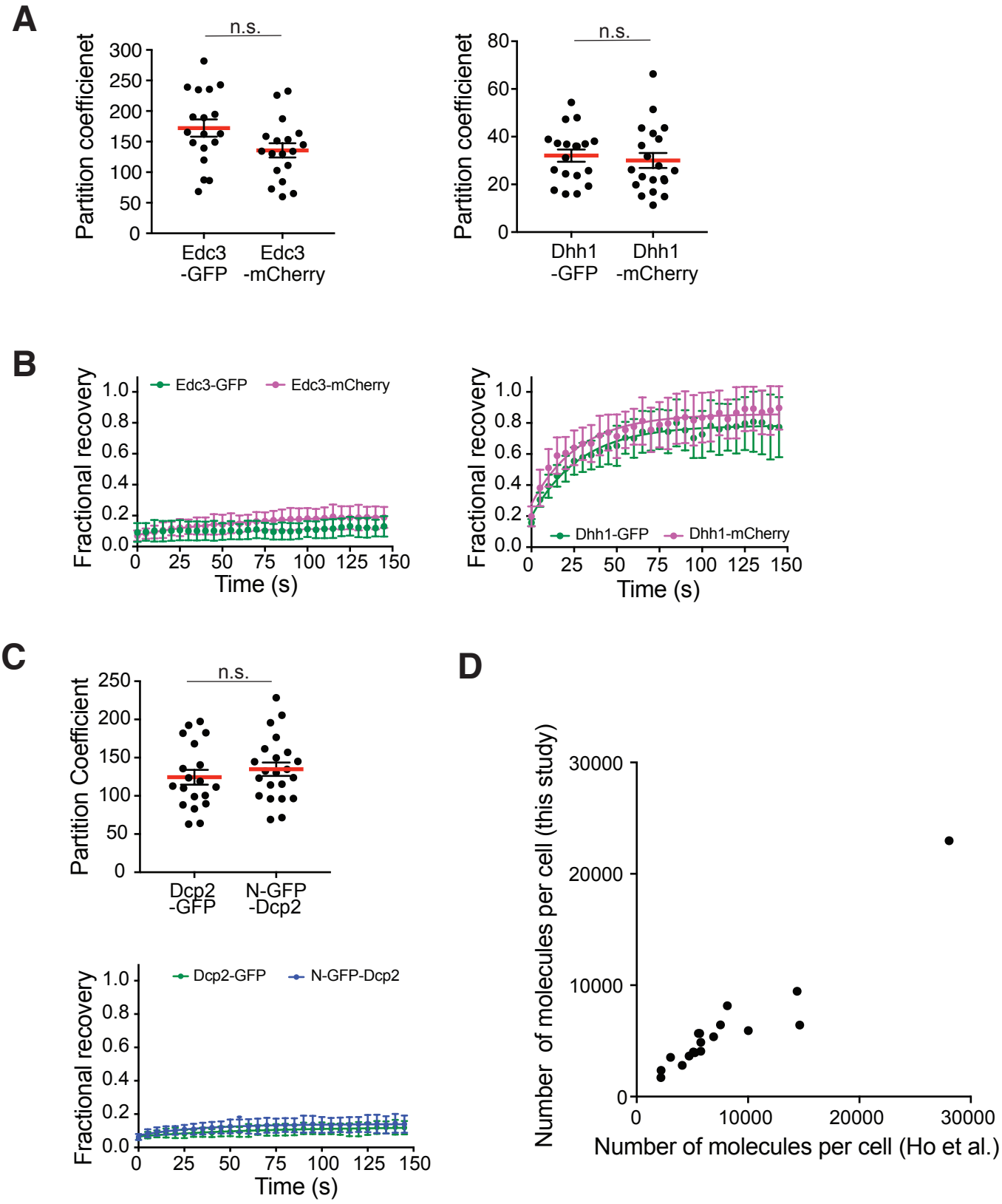

Figure 1 - figure supplement 4

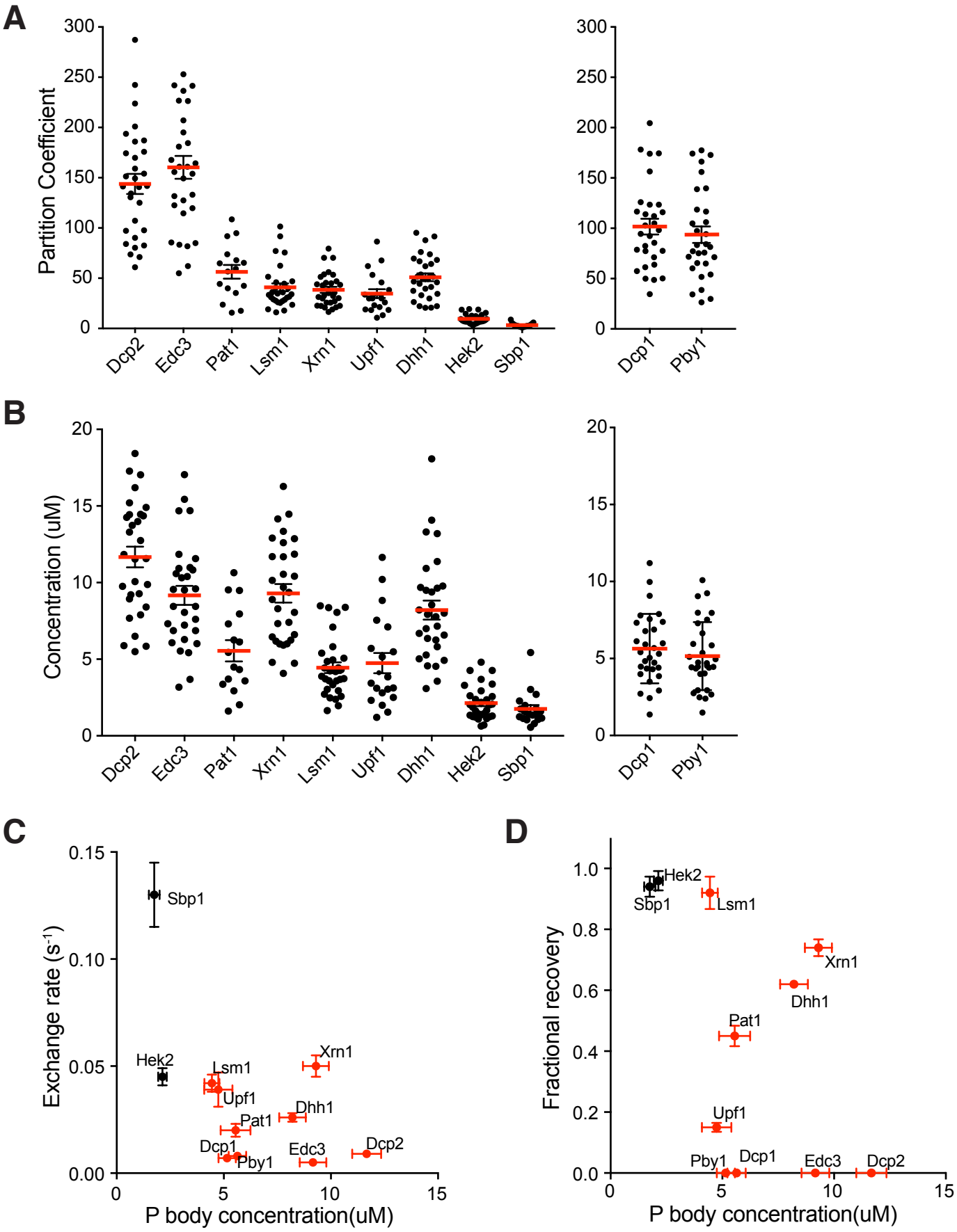

Figure 2

A

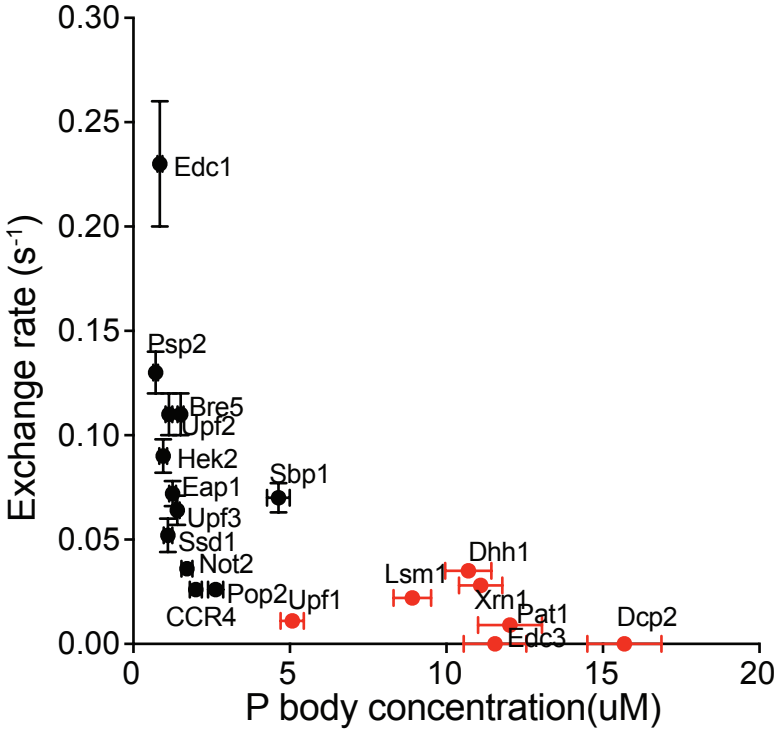
Exchange rate (s-1)
0.30
0.25
0.20
0.15
0.10
0.05
0.00
Edc1
Psp2
Bre5
Upf2
Hek2
Eap1
Sbp1
Upf3
Ssd1
Not2
Pop2
CCR4
Upf1
Lsm1
Dhh1
Xrn1
Pat1
Edc3
Dcp2
0
5
10
15
20
P body concentration(uM)

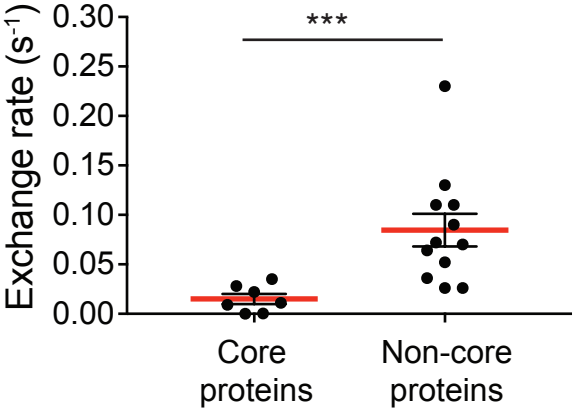
Exchange rate (s-1)
0.30
0.25
0.20
0.15
0.10
0.05
0.00
***
Core proteins
Non-core proteins

B

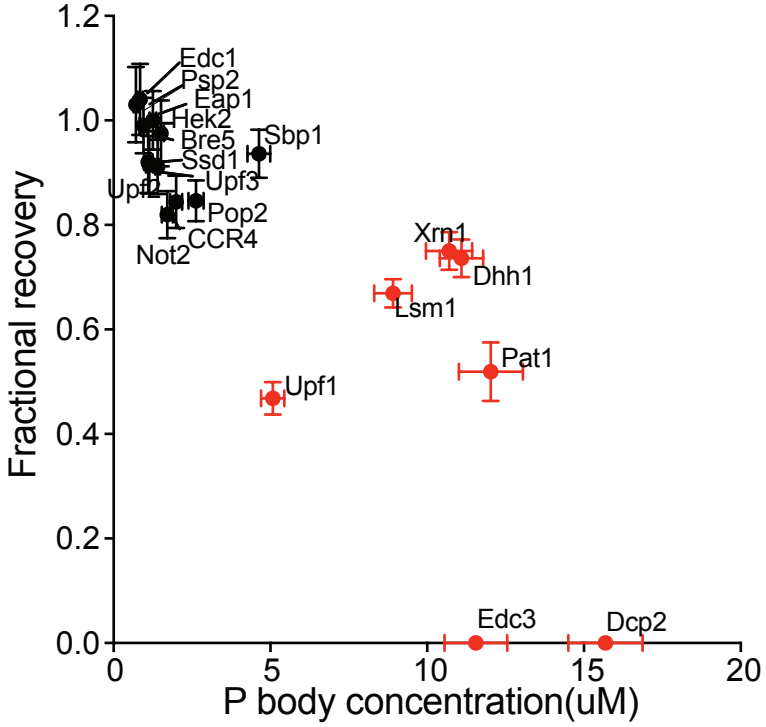
Fractional recovery
1.2
1.0
0.8
0.6
0.4
0.2
0.0
Edc1
Psp2
Eap1
Hek2
Bre5
Sbp1
Ssd1
Upf2
Upf3
Pop2
CCR4
Not2
Xrn1
Dhh1
Lsm1
Pat1
Upf1
Edc3
Dcp2
0
5
10
15
20
P body concentration(uM)

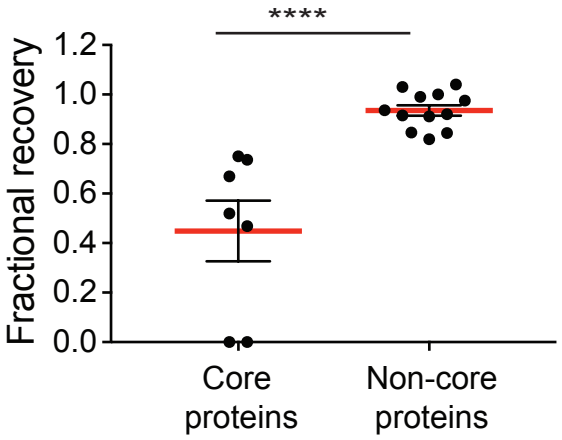
Fractional recovery
1.2
1.0
0.8
0.6
0.4
0.2
0.0
****
Core proteins
Non-core proteins

Figure 2 - figure supplement 1

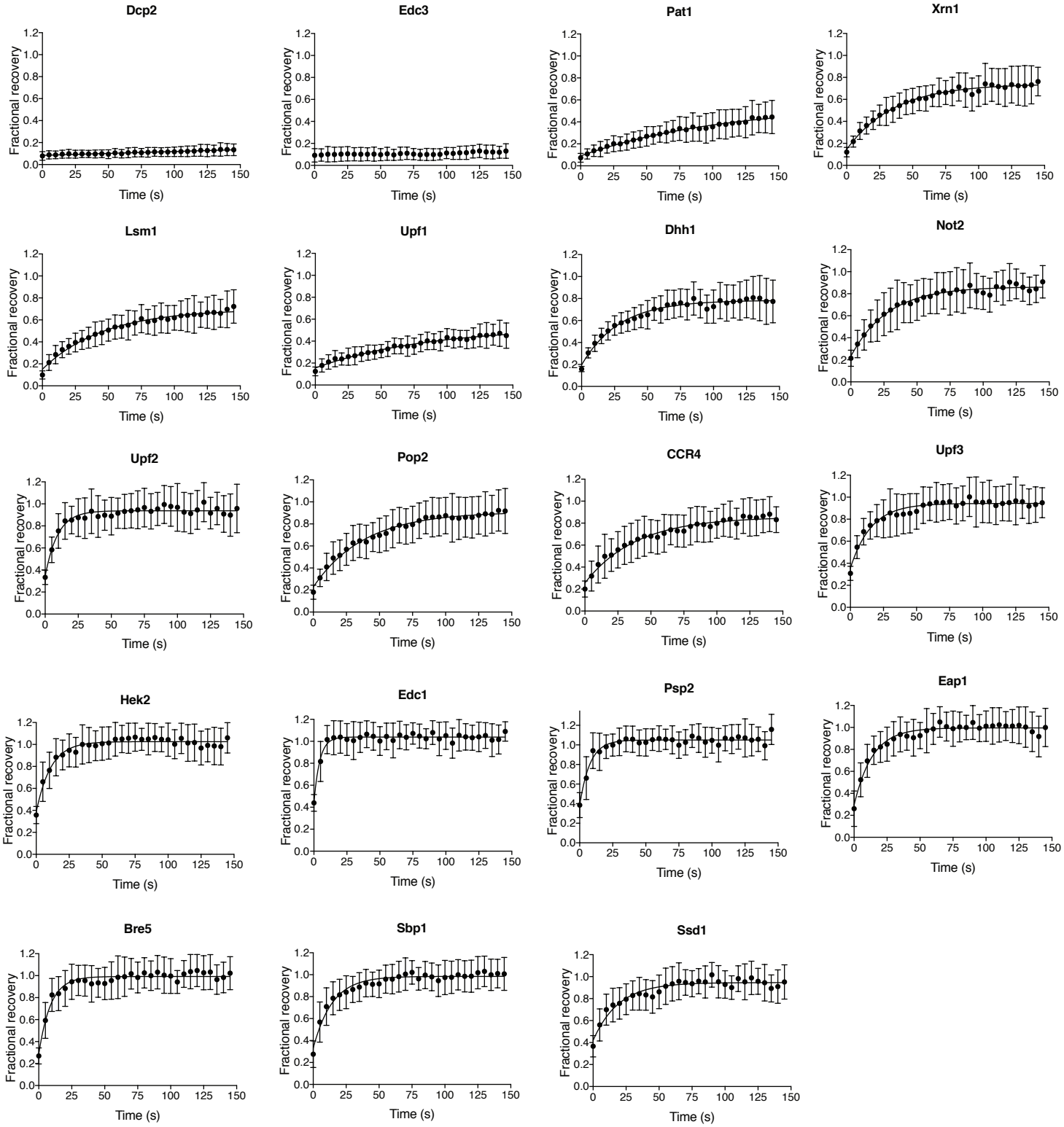

Figure 2 - figure supplement 2

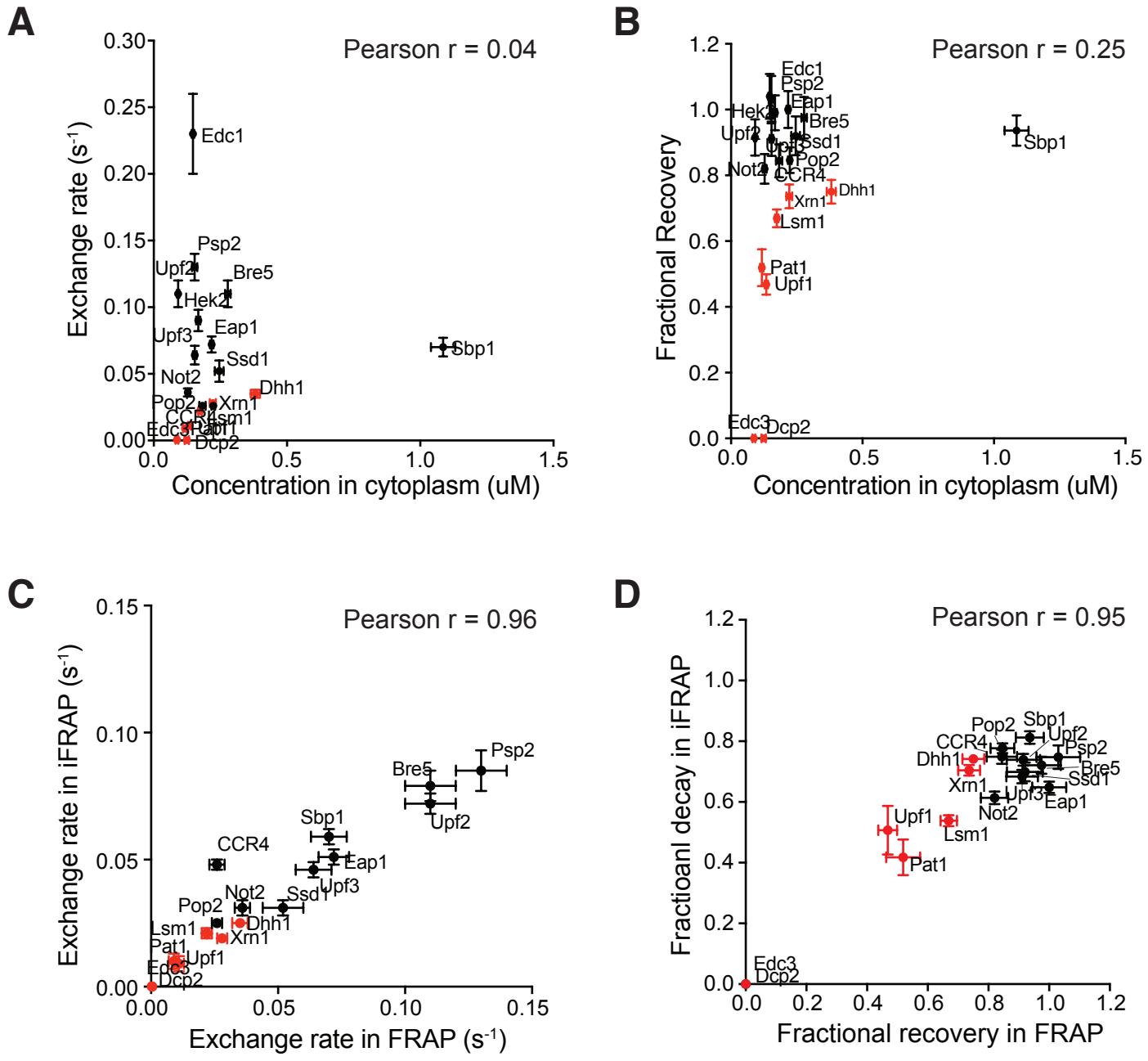

Figure 2 -figure supplement 3

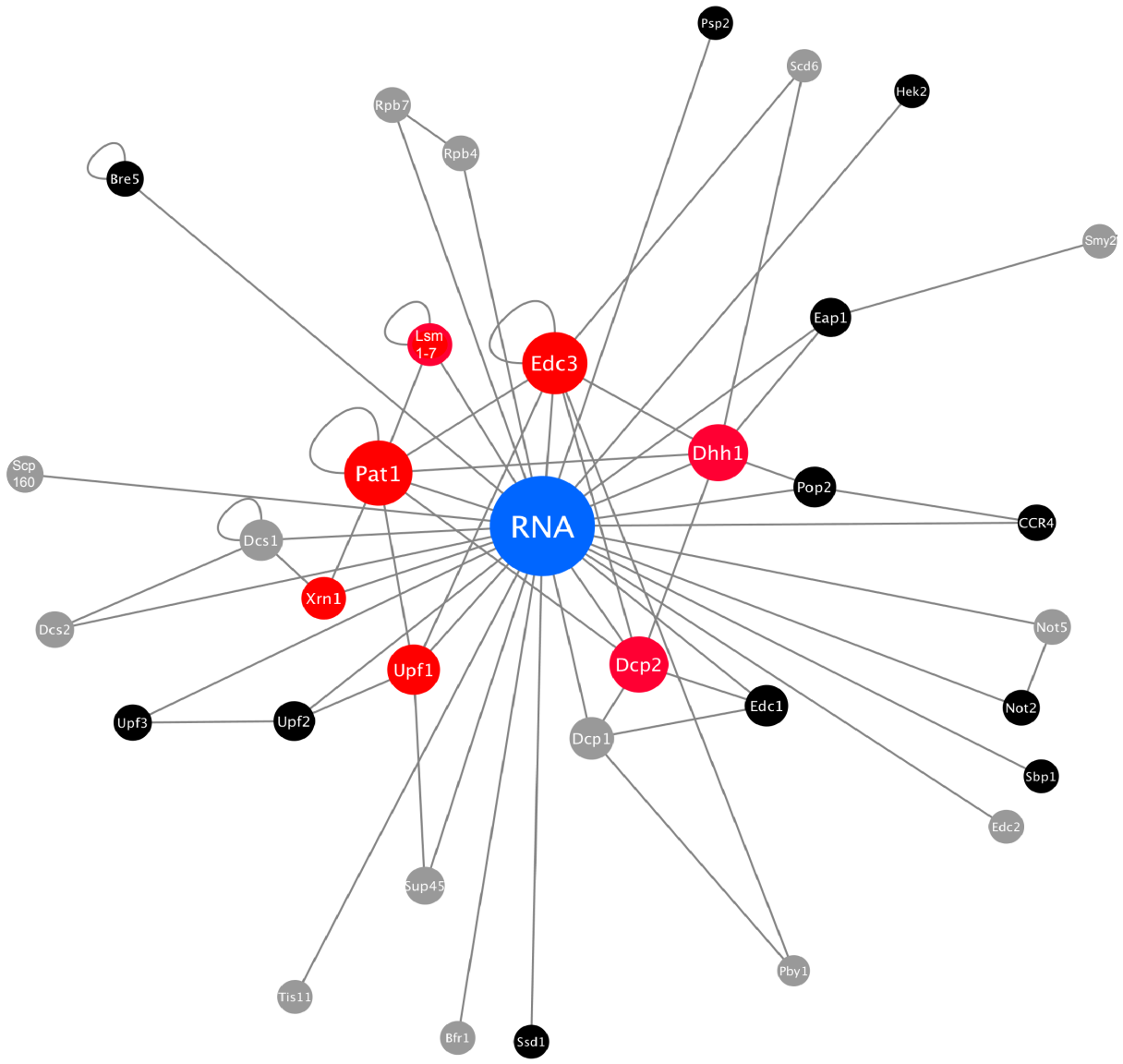

Figure 3

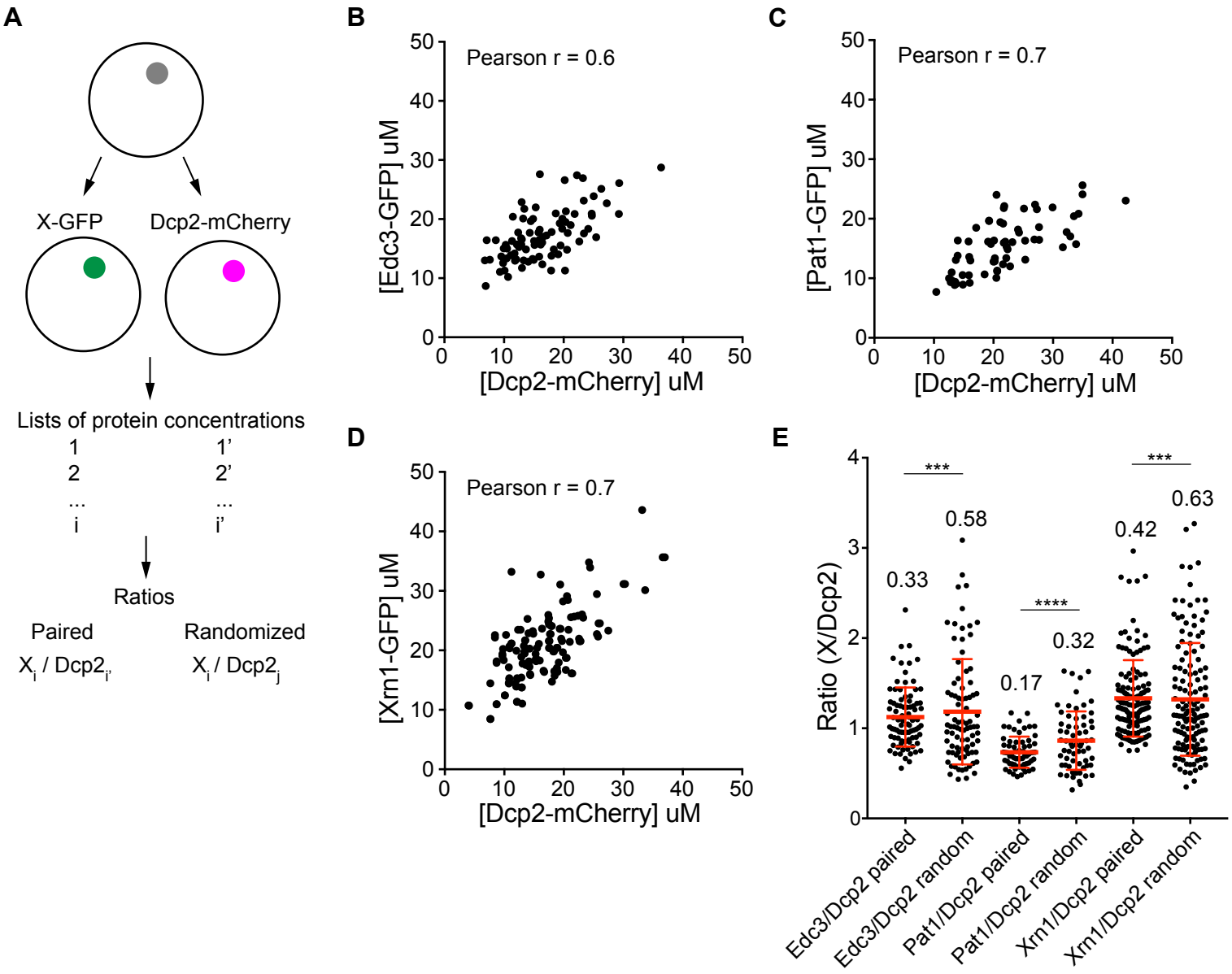
A
X-GFP
Dcp2-mCherry
Lists of protein concentrations
1
2
...
i
1'
2'
...
i'
Ratios
Paired
Randomized
X_i / $Dcp2_{i'}$
X_i / $Dcp2_j$
B
Pearson r = 0.6
[Edc3-GFP] uM
[Dcp2-mCherry] uM
C
Pearson r = 0.7
[Pat1-GFP] uM
[Dcp2-mCherry] uM
D
Pearson r = 0.7
[Xrn1-GFP] uM
[Dcp2-mCherry] uM
E
Ratio (X/Dcp2)
***
****
***
0.33
0.58
0.17
0.32
0.42
0.63
Edc3/Dcp2 paired
Edc3/Dcp2 random
Pat1/Dcp2 paired
Pat1/Dcp2 random
Xrn1/Dcp2 paired
Xrn1/Dcp2 random

Figure 4

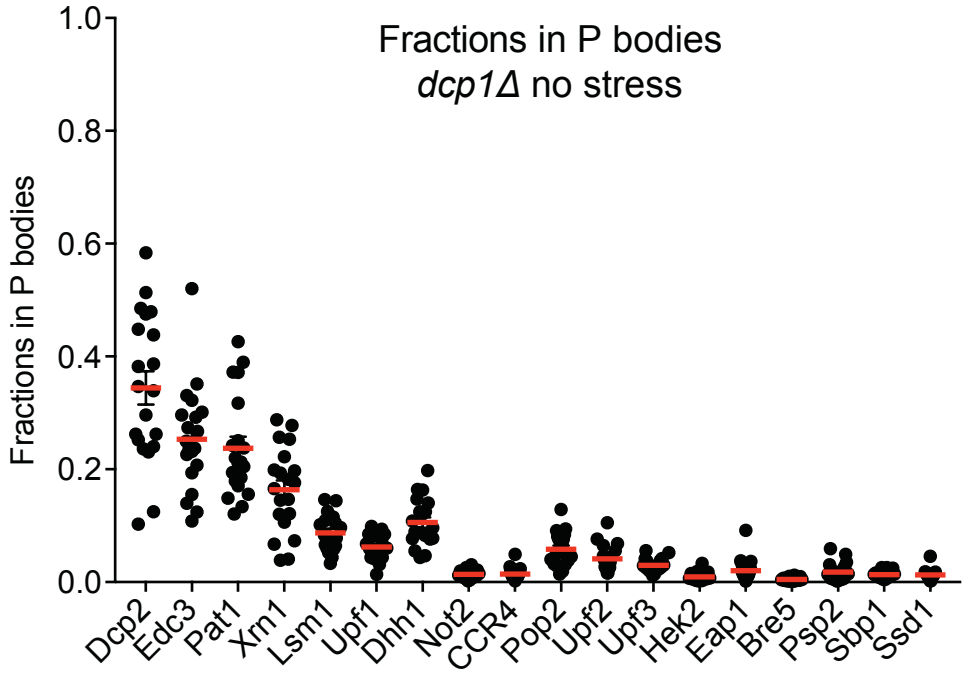
Fractions in P bodies
dcp1Δ no stress
Fractions in P bodies
1.0
0.8
0.6
0.4
0.2
0.0
Dcp2
Edc3
Pat1
Xrn1
Lsm1
Upf1
Dhh1
Not2
CCR4
Pop2
Upf2
Upf3
Hek2
Eap1
Bre5
Psp2
Sbp1
Ssd1

Figure 4 - figure supplement 1

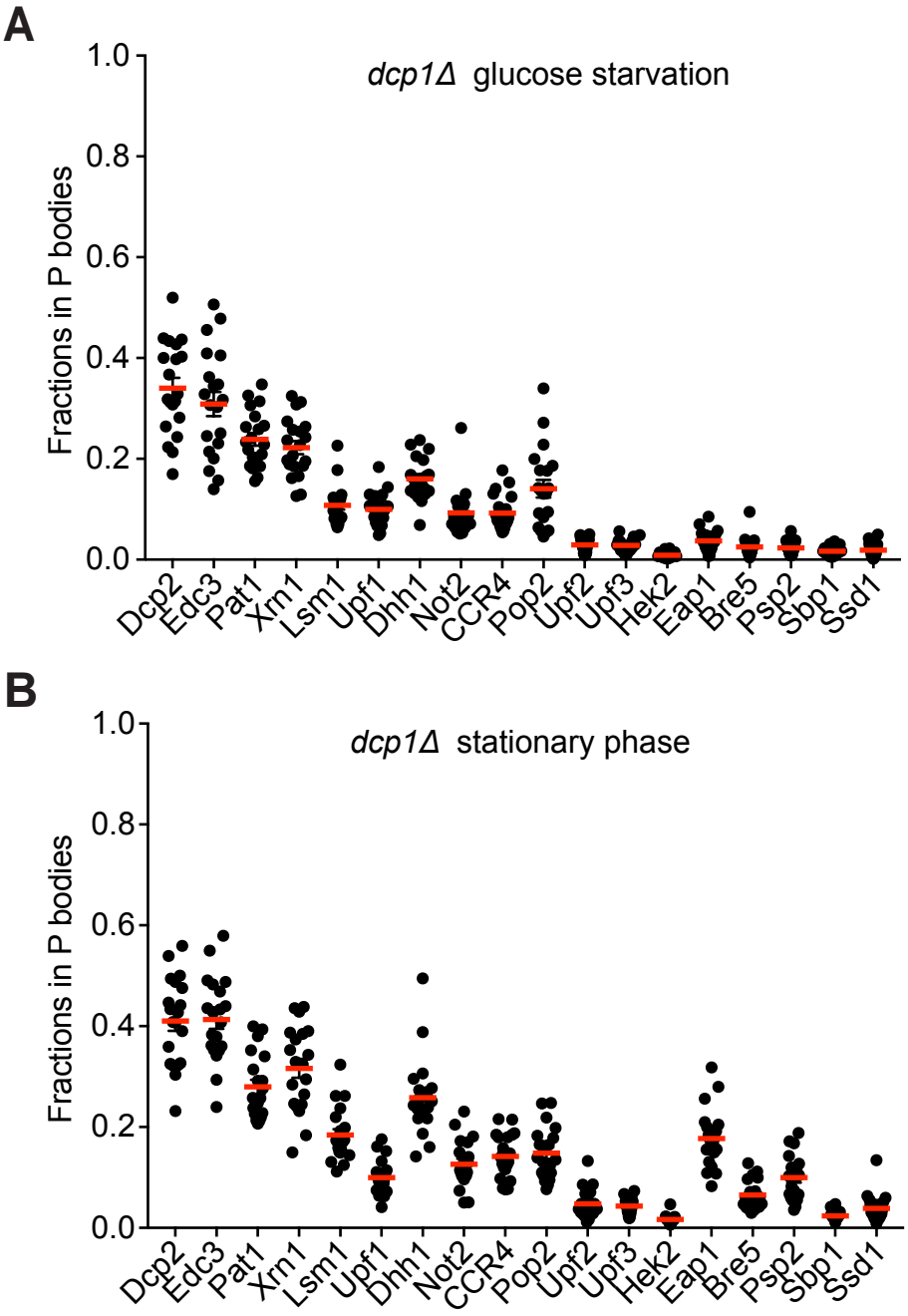

Figure 5

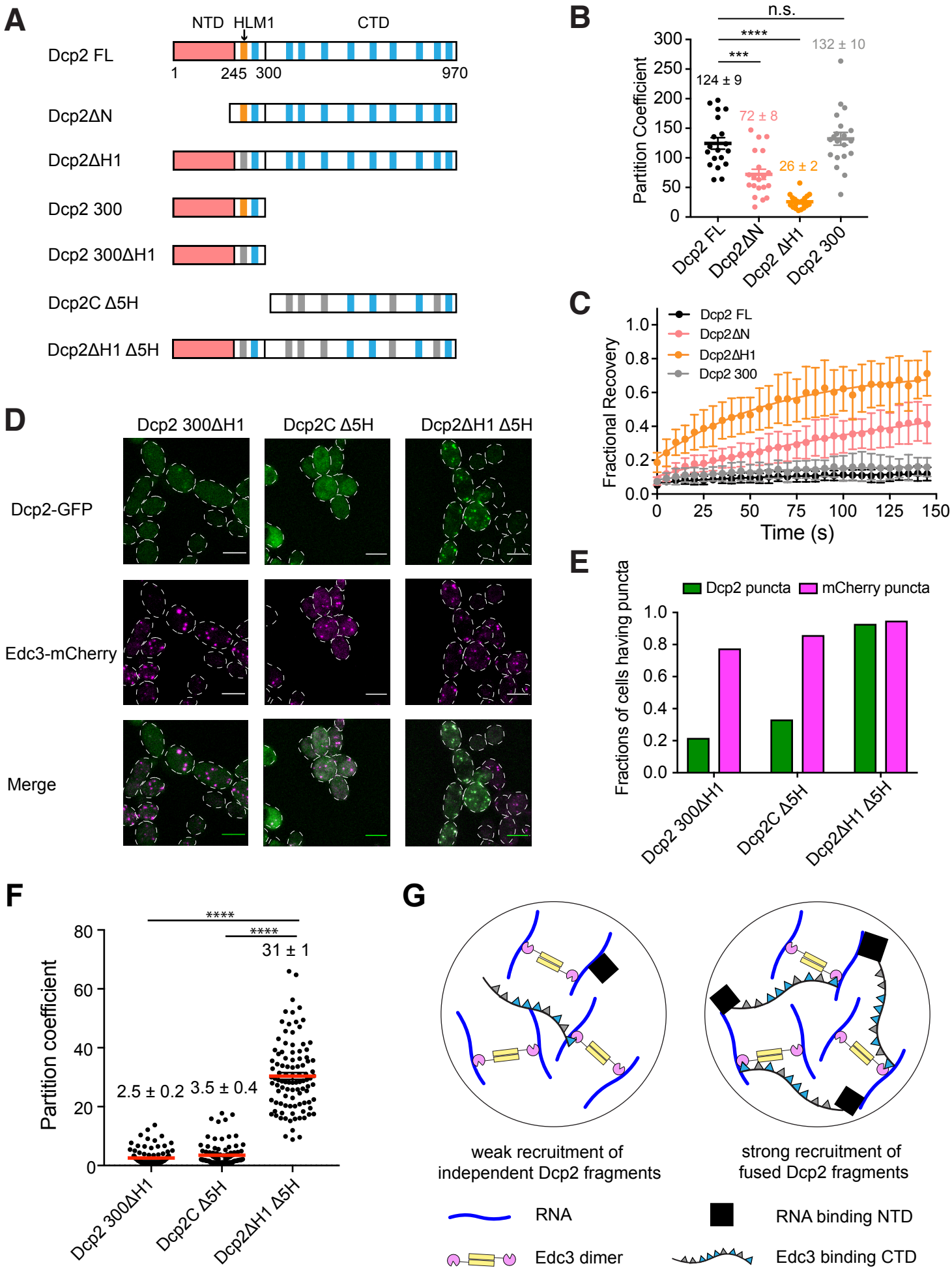
A
NTD
HLM1
CTD
Dcp2 FL
1
245
300
970
Dcp2ΔN
Dcp2ΔH1
Dcp2 300
Dcp2 300ΔH1
Dcp2C Δ5H
Dcp2ΔH1 Δ5H
B
n.s.
****
***
Partition Coefficient
124 ± 9
72 ± 8
26 ± 2
132 ± 10
Dcp2 FL
Dcp2ΔN
Dcp2 ΔH1
Dcp2 300
C
Dcp2 FL
Dcp2ΔN
Dcp2ΔH1
Dcp2 300
Fractional Recovery
Time (s)
D
Dcp2 300ΔH1
Dcp2C Δ5H
Dcp2ΔH1 Δ5H
Dcp2-GFP
Edc3-mCherry
Merge
E
Dcp2 puncta
mCherry puncta
Fractions of cells having puncta
Dcp2 300ΔH1
Dcp2C Δ5H
Dcp2ΔH1 Δ5H
F
****
****
Partition coefficient
2.5 ± 0.2
3.5 ± 0.4
31 ± 1
Dcp2 300ΔH1
Dcp2C Δ5H
Dcp2ΔH1 Δ5H
G
weak recruitment of
independent Dcp2 fragments
strong recruitment of
fused Dcp2 fragments
RNA
RNA binding NTD
Edc3 dimer
Edc3 binding CTD

Figure 5 - figure supplement 1

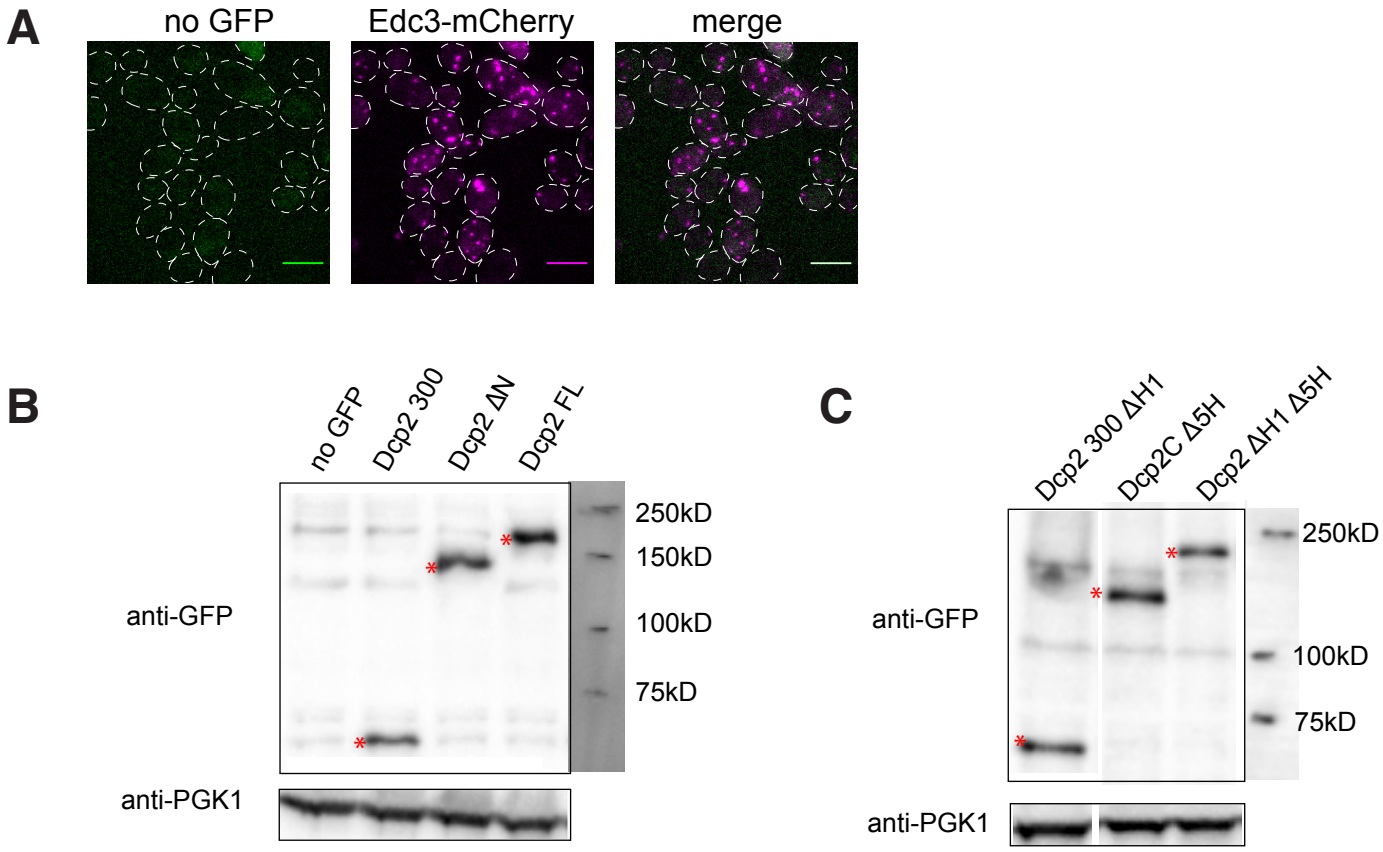

Figure 6

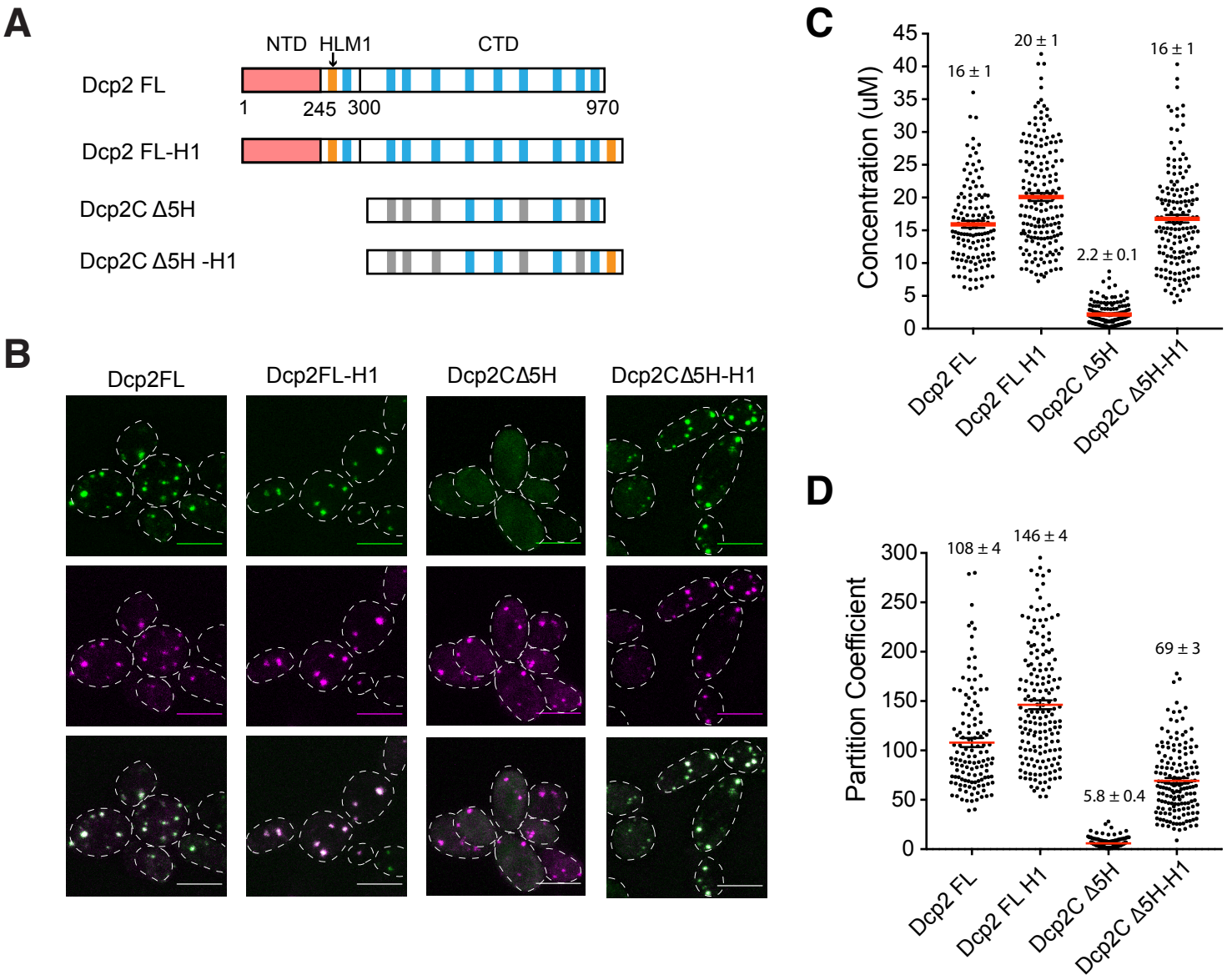
A
NTD
HLM1
CTD
Dcp2 FL
1
245
300
970
Dcp2 FL-H1
Dcp2C Δ5H
Dcp2C Δ5H -H1
B
Dcp2FL
Dcp2FL-H1
Dcp2CΔ5H
Dcp2CΔ5H-H1
C
Concentration (uM)
45
40
35
30
25
20
15
10
5
0
16 ± 1
20 ± 1
2.2 ± 0.1
16 ± 1
Dcp2 FL
Dcp2 FL H1
Dcp2C Δ5H
Dcp2C Δ5H-H1
D
Partition Coefficient
300
250
200
150
100
50
0
108 ± 4
146 ± 4
5.8 ± 0.4
69 ± 3
Dcp2 FL
Dcp2 FL H1
Dcp2C Δ5H
Dcp2C Δ5H-H1

Figure 6 - figure supplement 1

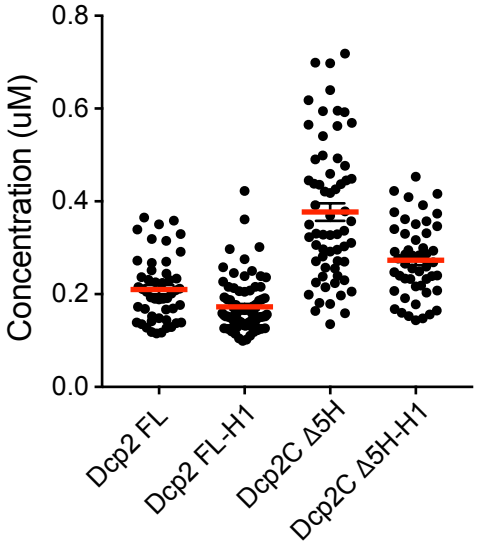

Figure 7

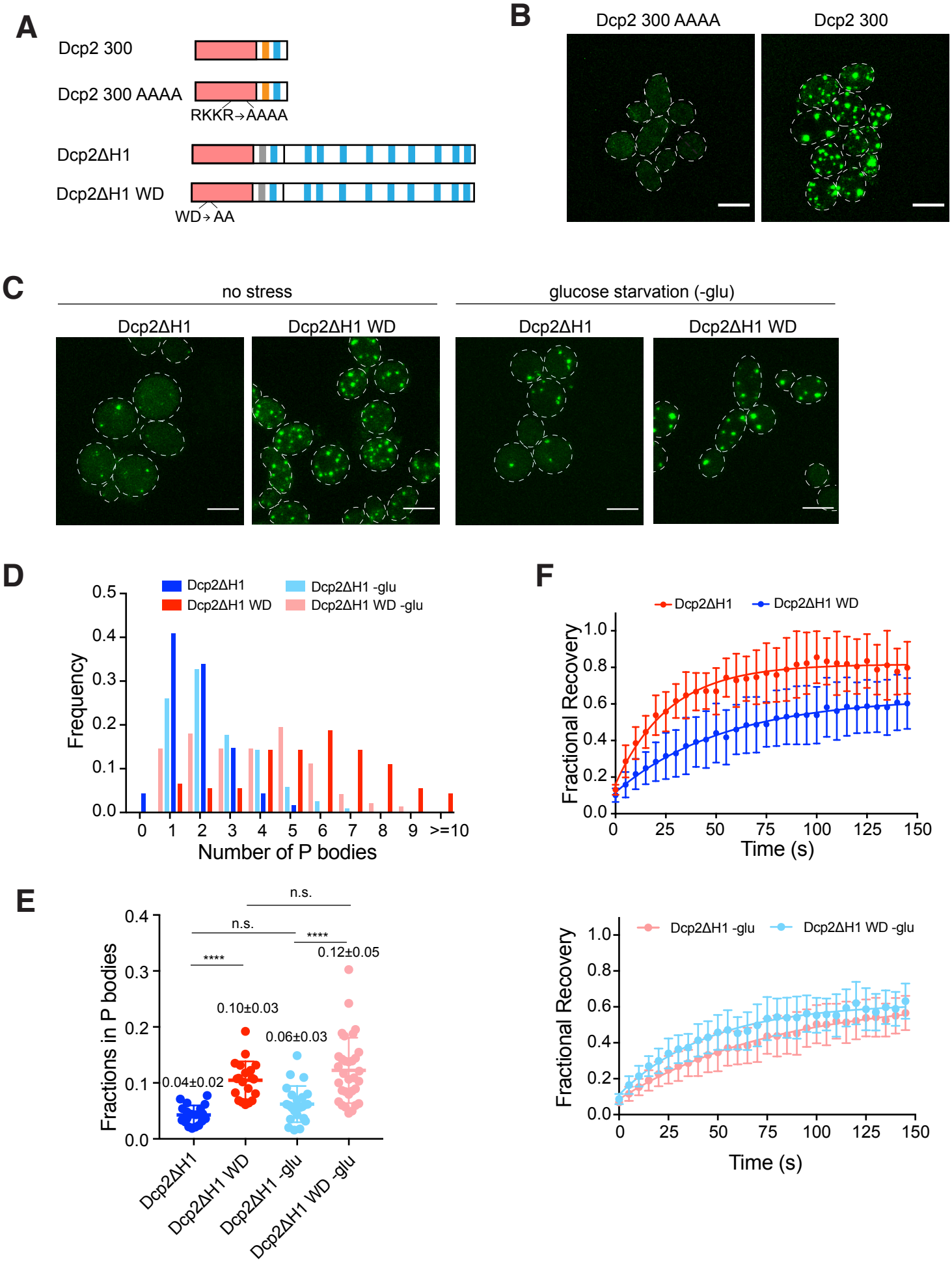
A
Dcp2 300
Dcp2 300 AAAA
RKKR→AAAA
Dcp2ΔH1
Dcp2ΔH1 WD
WD→AA
B
Dcp2 300 AAAA
Dcp2 300
C
no stress
glucose starvation (-glu)
Dcp2ΔH1
Dcp2ΔH1 WD
Dcp2ΔH1
Dcp2ΔH1 WD
D
Dcp2ΔH1
Dcp2ΔH1 WD
Dcp2ΔH1 -glu
Dcp2ΔH1 WD -glu
Frequency
Number of P bodies
0 1 2 3 4 5 6 7 8 9 >=10
F
Dcp2ΔH1
Dcp2ΔH1 WD
Fractional Recovery
Time (s)
E
n.s.
n.s.
****
****
0.12±0.05
0.10±0.03
0.06±0.03
0.04±0.02
Fractions in P bodies
Dcp2ΔH1
Dcp2ΔH1 WD
Dcp2ΔH1 -glu
Dcp2ΔH1 WD -glu
Dcp2ΔH1 -glu
Dcp2ΔH1 WD -glu
Fractional Recovery
Time (s)

Figure 7 - figure supplement 1

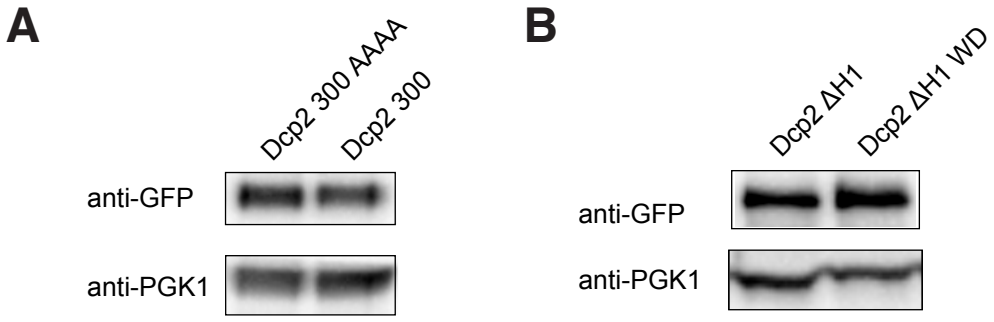

Table 1. Yeast strains used in this study

Yeast Strains	note	genotype	P body localization	Explanation for lacking of P body localization in *dcp1*Δ strain	Reference for strain	Reference for localization to P bodies
yRP3156	*dcp1*Δ *dcp2*Δ	*Mat a his4-539 leu2-3,112 lys2-201 trp1 ura3-52 dcp1::URA3(5FOA+) dcp2::TRP1 cup1::LEU2/PGK1pG/MFA2pG*			this study	
yRP1346	*dcp2*Δ	*Mat a his4-539 leu2-3,112 lys2-201 trp1 ura3-52 dcp2::TRP1 cup1::LEU2/PGK1pG/MFA2pG*			Dunckley and Parker 1999	
yRP1936	*dcp1*Δ Dcp2	*Mat a leu2-3,112 cup1::LEU2/PGK1pG/MFA2pG his4-539 trp1 ura3-52 DCP2-GFP(NEO) dcp1::URA3*	Y		Brengues et al 2005	Sheth and Parker 2003
yRP2254	*dcp1*Δ Edc3	*Mat a leu2-3,112 trp1 ura3-52 his4-539 lys2-201 cup1::LEU2/PGK1pG/MFA2pG dcp1::URA3 EDC3-GFP (NEO)*	Y		Teixeira et al 2007	Kshirsagar *et al* 2004
yRP2237	*dcp1*Δ Pat1	*Mat a leu2-3,112 trp1 ura3-52 his4-539 cup1::LEU2/PGK1pG/MFA2pG dcp1::URA3 PAT1-GFP (NEO)*	Y		Teixeira et al 2007	Sheth and Parker 2003
yRP2246	*dcp1*Δ Xrn1	*Mat a leu2-3,112 trp1 ura3-52 his4-539 cup1::LEU2/PGK1pG/MFA2pG dcp1::URA3 XRN1-GFP (NEO)*	Y		Teixeira et al 2007	Sheth and Parker 2003
yRP2230	*dcp1*Δ Lsm1	*Mat a leu2-3,112 trp1 ura3-52 his4-539 cup1::LEU2/PGK1pG/MFA2pG dcp1::URA3 LSM1-GFP (NEO)*	Y		Teixeira et al 2007	Sheth and Parker 2003
yRP1840	*dcp1*Δ Upf1	*Mat a leu2-3,112 trp1 ura3-52 his4-539 cup1::LEU2/PGK1pG/MFA2pG dcp1::URA3 UPF1-GFP (NEO)*	Y		Sheth and Parker 2006	Sheth and Parker 2006
yRP1736	*dcp1*Δ Dhh1	*Mat a leu2-3,112 trp1 ura3-52 his4-539 cup1::LEU2/PGK1pG/MFA2pG dcp1::URA3 DHH1-GFP (NEO)*	Y		Sheth and Parker 2003	Sheth and Parker 2003
yRP2269	*dcp1*Δ Pop2	*Mat a leu2-3,112 trp1 ura3-52 his4-539 cup1::LEU2/PGK1pG/MFA2pG dcp1::URA3 POP2-GFP (NEO)*	Y		Teixeira et al 2007	Sheth and Parker 2003, Teixeira *et al* 2007
yRP1844	*dcp1*Δ Upf3	*Mat a leu2-3.112 ura3-52 cup1::LEU2/PGK1pG/MFA2pG, dcp1::URA3, UPF3-GFP (NEO)*	Y		Sheth and Parker 2006	Sheth and Parker 2006
yRP1916	*dcp1*Δ Not2	*Mat alpha leu2-3,112 cup1::LEU2/PGK1pG/MFA2pG trp1 his4-539 ura3-52 dcp1::URA3 NOT2-GFP(NEO)*	Y		Muhlrad and Parker 2005	Sheth and Parker 2003, Teixeira *et al* 2007
yRP1842	*dcp1*Δ Upf2	*Mat a leu2-3,112, ura3-52 cup1::LEU2/PGK1pG/MFA2pG, dcp1:: URA3, UPF2-GFP(NEO)*	Y		Sheth and Parker 2006	Sheth and Parker 2006
yRP2261	*dcp1*Δ CCR4	*Mat a leu2-3,112 trp1 ura3-52 his4-539 cup1::LEU2/PGK1pG/MFA2pG dcp1::URA3 CCR4-GFP (NEO)*	Y		Teixeira et al 2007	Sheth and Parker 2003, Teixeira *et al* 2007
yRP3140	*dcp1*Δ Hek2	*Mat a leu2, ura3, his3, met15, dcp1::URA3 HEK2::GFP(HIS3MX6)*	Y		this study	Mitchell *et al* 2013
yRP3137	*dcp1*Δ Sbp1	*Mat alpha leu2, ura3, his3, met15, dcp1::URA3 SBP1::GFP(HIS3MX6)*	Y		this study	Mitchell et al 2013
yRP3154	*dcp1*Δ Edc1	*Mat a leu2, ura3, his3, met15, dcp1::URA3 EDC1::GFP(HIS3MX6)*	Y		this study	Neef *et al* 2009
yRP3143	*dcp1*Δ Bre5	*Mat a leu2, ura3, his3, met15, dcp1::URA3 BRE5::GFP(HIS3MX6)*	Y		this study	Mitchell *et al* 2013
yRP3136	*dcp1*Δ Psp2	*Mat a leu2, ura3, his3, met15, dcp1::URA3 PSP2::GFP(HIS3MX6)*	Y		this study	Mitchell *et al* 2013
yRP3146	*dcp1*Δ Eap1	*Mat a leu2, ura3, his3, met15, dcp1::URA3 EAP1::GFP(HIS3MX6)*	Y		this study	Mitchell *et al* 2013
yRP3149	*dcp1*Δ Ssd1	*Mat a leu2, ura3, his3, met15, dcp1::URA3 SSD1::GFP(HIS3MX6)*	Y		this study	Kurischko *et al* 2011
yRP1919	*dcp1*Δ Not5	*Mat alpha trp1 leu2-3, 112 cup1::LEU2/PGK1pG/MFA2pG ura3-52 dcp1::URA3 NOT5-GFP(NEO)*	N		Muhlrad and Parker 2005	Sheth and Parker 2003, Teixeira *et al* 2007
yRP3083	*dcp1*Δ Scd6	*Mat alpha leu2, ura3, his3, met15, dcp1::URA3 SCD6::GFP(HIS3MX6)*	N	Compete binding sites on Dcp2 with Edc3. Because Edc3 is highly concentrated, Scd6 partitioning can be very poor.	this study	Rajyaguru *et al* 2012
yRP3142	*dcp1*Δ Brf1	*Mat alpha leu2, ura3, his3, met15, dcp1::URA3 BFR1::GFP(HIS3MX6)*	N	Reported to localize to P bodies after 50min - glucose. Might be stress specific	this study	Simpson *et al* 2014
yRP3144	*dcp1*Δ Dcs1	*Mat alpha leu2, ura3, his3, met15, dcp1::URA3 DCS1::GFP(HIS3MX6)*	N	P body localization is not shown by microscope	this study	Malys *et al* 2006
yRP3145	*dcp1*Δ Dcs2	*Mat alpha leu2, ura3, his3, met15, dcp1::URA3 DCS2::GFP(HIS3MX6)*	N	Dcs2 is reported to locate in P bodies as cells progressed into diauxie. We only analyzed log-phase cells.	this study	Malys *et al* 2006
yRP3139	*dcp1*Δ Edc2	*Mat alpha leu2, ura3, his3, met15, dcp1::URA3 EDC2::GFP(HIS3MX6)*	N	A subset of it is reported to localize to P bodies under glucose starvation or del_Xrn1 strains. Maybe stress specific.	this study	Neef *et al* 2009
yRP3141	*dcp1*Δ Rbp4	*Mat alpha leu2, ura3, his3, met15, dcp1::URA3 RBP4::GFP(HIS3MX6)*	N	P body localization increased after 4h starvation (lacking both glucose and amino acid) and increased more after 24 stravation. May be stress specific.	this study	Lotan *et al* 2005
yRP3153	*dcp1*Δ Rbp7	*Mat alpha leu2, ura3, his3, met15, dcp1::URA3 RBP7::GFP(HIS3MX6)*	N	Rpb7 co-localizes with Dcp2 after long starvation. May be stress specific	this study	Lotan *et al* 2007
yRP3150	*dcp1*Δ Sup45	Mat a ura3 his3 leu2 met15 dcp1Δ::URA3 SUP45::GFP(HIS3MX6)	N		this study	Buchan *et al* 2008
yRP3148	*dcp1*Δ Smy2	*Mat a leu2, ura3, his3, met15, dcp1::URA3 SMY2::GFP(HIS3MX6)*	N	Localization of P body was found using transfected plasmid. May be partition into P bodies when overexpressed.	this study	Georgiev *et al* 2007

yRP3147	*dcp1Δ* Tis11	*Mat a leu2, ura3, his3, met15, dcp1::URA3 TIS11::GFP(HIS3MX6)*	N	Binds to 3'UTR of specific mRNAs and partition into P bodies when expressing on plasmid. May be overexpressed, or the specific mRNAs are not in P bodies under our experimental conditions.	this study	Pedro-Segura *et al* 2008
yRP3138	*dcp1Δ* Pby1	*Mat a leu2, ura3, his3, met15, dcp1::URA3 PBY1::GFP(HIS3MX6)*	N	Pby1 is reported to interact with Dcp1. Lacking the factor recruiting Pby1 into P bodies in dcp1Δ strain.	this study	Sweet *et al* 2007
RESGEN	WT Dcp2	MATa his3Δ leu2Δ met15Δ ura3Δ DCP2::GFP(HIS3MX6)	Y		Huh et al., 2003	Sheth and Parker 2003
RESGEN	WT Edc3	MATa his3Δ leu2Δ met15Δ ura3Δ EDC3::GFP(HIS3MX6)	Y		Huh et al., 2003	Kshirsagar *et al* 2004
RESGEN	WT Pat1	MATa his3Δ leu2Δ met15Δ ura3Δ PAT1::GFP(HIS3MX6)	Y		Huh et al., 2003	Sheth and Parker 2003
RESGEN	WT Xrn1	MATa his3Δ leu2Δ met15Δ ura3Δ XRN1::GFP(HIS3MX6)	Y		Huh et al., 2003	Sheth and Parker 2003
RESGEN	WT Lsm1	MATa his3Δ leu2Δ met15Δ ura3Δ LSM1::GFP(HIS3MX6)	Y		Huh et al., 2003	Sheth and Parker 2003
RESGEN	WT Upf1	MATa his3Δ leu2Δ met15Δ ura3Δ UPF1::GFP(HIS3MX6)	Y		Huh et al., 2003	Sheth and Parker 2006
RESGEN	WT Dhh1	MATa his3Δ leu2Δ met15Δ ura3Δ DHH1::GFP(HIS3MX6)	Y		Huh et al., 2003	Sheth and Parker 2003
RESGEN	WT Pop2	MATa his3Δ leu2Δ met15Δ ura3Δ POP2::GFP(HIS3MX6)	N		Huh et al., 2003	Sheth and Parker 2003, Teixeira *et al* 2007
RESGEN	WT Upf3	MATa his3Δ leu2Δ met15Δ ura3Δ UPF1::GFP(HIS3MX6)	N		Huh et al., 2003	Sheth and Parker 2006
RESGEN	WT Not2	MATa his3Δ leu2Δ met15Δ ura3Δ NOT2::GFP(HIS3MX6)	N		Huh et al., 2003	Sheth and Parker 2003, Teixeira *et al* 2007
RESGEN	WT Upf2	MATa his3Δ leu2Δ met15Δ ura3Δ UPF2::GFP(HIS3MX6)	N		Huh et al., 2003	Sheth and Parker 2006
RESGEN	WT CCR4	MATa his3Δ leu2Δ met15Δ ura3Δ CCR4::GFP(HIS3MX6)	N		Huh et al., 2003	Sheth and Parker 2003, Teixeira *et al* 2007
RESGEN	WT Hek2	MATa his3Δ leu2Δ met15Δ ura3Δ HEK2::GFP(HIS3MX6)	Y		Huh et al., 2003	Mitchell *et al* 2013
RESGEN	WT Sbp1	MATa his3Δ leu2Δ met15Δ ura3Δ SBP1::GFP(HIS3MX6)	Y		Huh et al., 2003	Mitchell et al 2013
RESGEN	WT Edc1	MATa his3Δ leu2Δ met15Δ ura3Δ EDC1::GFP(HIS3MX6)	N		Huh et al., 2003	Neef *et al* 2009
RESGEN	WT Bre5	MATa his3Δ leu2Δ met15Δ ura3Δ BRE5::GFP(HIS3MX6)	N		Huh et al., 2003	Mitchell *et al* 2013
RESGEN	*WT* Psp2	MATa his3Δ leu2Δ met15Δ ura3Δ PSP2::GFP(HIS3MX6)	N		Huh et al., 2003	Mitchell *et al* 2013
RESGEN	WT Eap1	MATa his3Δ leu2Δ met15Δ ura3Δ EAP1::GFP(HIS3MX6)	N		Huh et al., 2003	Buchan *et al* 2008
RESGEN	WT Ssd1	MATa his3Δ leu2Δ met15Δ ura3Δ SSD1::GFP(HIS3MX6)	N		Huh et al., 2003	Kurischko *et al* 2011
RESGEN	WT Not5	MATa his3Δ leu2Δ met15Δ ura3Δ NOT5::GFP(HIS3MX6)	N		Huh et al., 2003	Sheth and Parker 2003, Teixeira *et al* 2007
RESGEN	WT Scd6	MATa his3Δ leu2Δ met15Δ ura3Δ SCD6::GFP(HIS3MX6)	N		Huh et al., 2003	Rajyaguru *et al* 2012
RESGEN	WT Brf1	MATa his3Δ leu2Δ met15Δ ura3Δ BRF1::GFP(HIS3MX6)	N		Huh et al., 2003	Simpson *et al* 2014
RESGEN	WT Dcs1	MATa his3Δ leu2Δ met15Δ ura3Δ DCS1::GFP(HIS3MX6)	N		Huh et al., 2003	Malys *et al* 2006
RESGEN	WT Dcs2	MATa his3Δ leu2Δ met15Δ ura3Δ DCS2::GFP(HIS3MX6)	N		Huh et al., 2003	Malys *et al* 2006
RESGEN	WT Edc2	MATa his3Δ leu2Δ met15Δ ura3Δ EDC2::GFP(HIS3MX6)	N		Huh et al., 2003	Neef *et al* 2009
RESGEN	WT Rbp4	MATa his3Δ leu2Δ met15Δ ura3Δ RPB4::GFP(HIS3MX6)	N		Huh et al., 2003	Lotan *et al* 2005
RESGEN	WT Rbp7	MATa his3Δ leu2Δ met15Δ ura3Δ RBP7::GFP(HIS3MX6)	N		Huh et al., 2003	Lotan *et al* 2007
RESGEN	WT Sup45	MATa his3Δ leu2Δ met15Δ ura3Δ RBP7::GFP(HIS3MX6)	N		Huh et al., 2003	Buchan *et al* 2008
RESGEN	WT Smy2	MATa his3Δ leu2Δ met15Δ ura3Δ SMY2::GFP(HIS3MX6)	N		Huh et al., 2003	Georgiev *et al* 2007
RESGEN	WT Tis11	MATa his3Δ leu2Δ met15Δ ura3Δ TIS11::GFP(HIS3MX6)	N		Huh et al., 2003	Pedro-Segura *et al* 2008
RESGEN	WT Pby1	MATa his3Δ leu2Δ met15Δ ura3Δ PBY1::GFP(HIS3MX6)	Y		Huh et al., 2003	Sweet *et al* 2007
RESGEN	WT Dcp1	MATa his3Δ leu2Δ met15Δ ura3Δ DCP1::GFP(HIS3MX6)	Y		Huh et al., 2003	Sheth and Parker 2003
yRP3239	*dcp1Δ* Dcp2-mCherry, Edc3-GFP	MAT alpha lys2 leu2-3,112 trp1 ura3-52 his4-539 cup1::LEU2/PGK1pG/MFA2pG dcp1::URA3 DCP2mCH:HYGB EDC3GFPNEO	Y		this study	
yRP3238	*dcp1Δ* Dcp2-mCherry, Pat1-GFP	MAT alpha lys2 leu2-3,112 trp1 ura3-52 his4-539 cup1::LEU2/PGK1pG/MFA2pG dcp1::URA3 DCP2mCH:HYGB PAT1GFPNEO	Y		this study	
yRP3240	*dcp1Δ* Dcp2-mCherry, Xrn1-GFP	MAT alpha lys2 leu2-3,112 trp1 ura3-52 his4-539 cup1::LEU2/PGK1pG/MFA2pG dcp1::URA3 DCP2mCH:HYGB XRN1GFPNEO	Y		this study	

Table 2. Dynamics and partitioning of P body proteins*

Proteins	Partition Coefficient	P body concentrations (uM)	Cytoplasm concentrations (uM)	Exchange rate (s^{-1})**	Fractional recovery
Dcp2	133 ± 13	15 ± 1	0.12 ± 0.01	~ 0.0003***	0
Edc3	133 ± 8	12 ± 1	0.09 ± 0.01	~ 0.0005***	0
Pat1	107 ± 12	12 ± 1	0.12 ± 0.01	0.009 ± 0.002	0.52 ± 0.06
Xrn1	53 ± 3	11 ± 1	0.22 ± 0.01	0.028 ± 0.002	0.74 ± 0.04
Lsm1	52 ± 4	8.9 ± 0.6	0.17 ± 0.01	0.022 ± 0.002	0.67 ± 0.03
Upf1	39 ± 3	5.1 ± 0.4	0.13 ± 0.01	0.011 ± 0.002	0.47 ± 0.03
Dhh1	30 ± 2	10 ± 1	0.38 ± 0.02	0.035 ± 0.003	0.75 ± 0.04
Not2	14 ± 1	1.7 ± 0.2	0.13 ± 0.01	0.036 ± 0.003	0.82 ± 0.05
CCR4	13 ± 1	2.0 ± 0.2	0.18 ± 0.01	0.026 ± 0.003	0.84 ± 0.05
Pop2	12 ± 1	2.6 ± 0.2	0.22 ± 0.01	0.026 ± 0.002	0.85 ± 0.04
Upf2	12 ± 1	1.1 ± 0.1	0.09 ± 0.01	0.11 ± 0.01	0.92 ± 0.06
Upf3	9.6 ± 0.8	1.4 ± 0.1	0.15 ± 0.01	0.064 ± 0.007	0.91 ± 0.05
Hek2	5.9 ± 0.8	1.0 ± 0.1	0.16 ± 0.01	0.091 ± 0.008	0.99 ± 0.05
Eap1	5.8 ± 0.5	1.2 ± 0.1	0.22 ± 0.01	0.072 ± 0.006	1.00 ± 0.06
Edc1	5.7 ± 0.5	0.8 ± 0.1	0.15 ± 0.01	0.23 ± 0.03	1.00 ± 0.07
Bre5	5.6 ± 0.4	1.5 ± 0.1	0.28 ± 0.01	0.11 ± 0.01	0.97 ± 0.06
Psp2	4.8 ± 0.5	0.7 ± 0.1	0.15 ± 0.01	0.13 ± 0.01	1.00 ± 0.07
Sbp1	4.5 ± 0.4	4.6 ± 0.4	1.1 ± 0.05	0.069 ± 0.007	0.94 ± 0.05
Ssd1	4.5 ± 0.4	1.1 ± 0.1	0.25 ± 0.02	0.052 ± 0.008	0.92 ± 0.06

* Mean ± SEM for partitioning coefficient, P body concentrations, Cytoplasm concentrations, Exchange rate and Fractional recovery.
** Exchange rate is exponential rate constant of exchange (k).
*** FRAP curves of Dcp2 and Edc3 are almost flat that the software can only fit ambiguous values.

Table 3. Protein-Protein and Protein-RNA interactions among P body proteins

	Protein-protein interactions	Protein-RNA interactions	Total types of interacting molecules	Total interactions	Core or non-core protein in this study	Effect on P bodies when deleted	References
Dcp2	Edc3 + Pat1(10 in total), Dhh1, Edc1, Dcp1	1	6	14	Core	Increased number when deleted alone, but smaller size than *dcp1*Δ. Smaller size in *dcp1*Δ*dcp2*Δ	Harigaya et al., 2010, Decker et al., 2007; Nissan et al., 2010; Dunckley et al., 2001; Charenton et al., 2017; Teixeira et al., 2007
Edc3	Dcp2, Edc3, Dhh1, Upf1, Pat1,Pby1, Scd6	>=1	8	>=8	Core	Decreased number	Harigaya et al., 2010, Decker et al., 2007, Swisher et al., 2011; Pilkington and Parker, 2008
Pat1	Pat1, Dcp2/Xrn1 (same site), Dhh1, Edc3, Lsm1-7, Upf1	1	8	8	Core	Smaller size	Nissan et al., 2010, Swisher et al., 2011; Pilkington and Parker, 2008; Sheth et al., 2003; Teixeira et al., 2007
Xrn1	Pat1, Dcs1	1	3	3	Core	Increased number	Nissan et al., 2010, Sheth et al., 2003
Lsm1-7	Pat1, Lsm4 Q/N domain (>=1)	1+1	3	4	Core	Decreased number when *edc3*Δ	Decker et al., 2007, Sharif and Conti, 2013; Decker et al., 2007
Upf1	Pat1, Edc3, Upf2, Sup45	1	5	5	Core	No effect	Swisher et al., 2011, Sheth et al., 2006
Dhh1	Pat1/Edc3 (same site), Dcp2, (Pop2), (Eap1)	>=1	6	5	Core	No effect	Nissan et al., 2010, Decker et al., 2007; Blewett and Goldstrohm, 2012; Coller et al., 2001; Rao and Parker, 2017
Pop2	CCR4, (Dhh1)	1	3	3	non-core	n.d.	Coller et al., 2001, Basquin et al., 2012;; Sheth et al 2003, Teixeira et al 2007
CCR4	Pop2	1	2	2	non-core	No effect	Basquin et al., 2012, Teixeira et al., 2007
Not2	Not5	1	2	2	non-core	n.d.	Bhaskar et al., 2013, Sheth et al 2003, Teixeira et al 2007
Upf3	Upf2	1	2	2	non-core	Increased number	He et al., 1997, Sheth et al., 2006
Upf2	Upf1, Upf3	1	3	3	non-core	Increased number	Swisher et al., 2011, Sheth et al., 2006
Hek2		>=1	1	>=1	non-core	n.d.	Irie et al., 2002, Mitchell et al., 2003
Sbp1		>=1	1	>=1	non-core	Smaller size in *sbp1*Δ when grow to higher OD	Mitchell et al., 2013, Segal et al., 2006
Edc1	Dcp2, Dcp1	1	3	3	non-core	n.d.	Schwartz et al., 2003, Neef et al., 2009, Borja
Bre5	Bre5	1	2	2	non-core	n.d.	Li et al., 2005, Mitchell et al., 2013
Psp2		1	1	1	non-core	n.d.	Mitchell et al., 2013, Rao and Parker, 2017
Eap1	(Dhh1), (Smy2)	1	3	3	non-core	n.d.	Blewett and Goldstrohm., 2012, Mitchell et al., 2013
Ssd1		1	1	1	non-core	n.d.	Uesono et al., 1997, Kurischko et al., 2013
Scd6	Edc3, Dhh1		2	2	non-core	n.d.	Nissan et al., 2008
Not5	Not2	1	2	2	non-core	n.d.	Bhaskar et al., 2013, Sheth et al 2003, Teixeira et al 2007
Bfr1		1	1	1	non-core	increased number	Mitchell et al., 2013, Weidner et al., 2014
Scp160		1	1	1	non-core	increased number	Weidner et al., 2014
Dcs1	Xrn1, Dcs2, Dcs1	1	4	4	non-core	n.d.	Sinture et al., 2012, Malys et al, 2006
Dcs2	Dcs1	1	2	2	non-core	n.d.	Malys et al., 2006
Edc2		1	1	1	non-core	n.d.	Schwartz et al., 2003
Rpb4	Rpb7	1	2	2	non-core	increased number	Lotan et al., 2005, Armache et al., 2003

Rpb7	Rpb4	1	2	2	non-core	same number of P bodies after heat stress, while in WT cells, number of P bodies decreased.	Armache et al., 2003, Lotan et al., 2007
Sup45	Upf1	1	2	2	non-core	n.d.	Czaplinski et al., 1998
Smy2	(Eap1)		1	(1)	non-core	n.d.	Kofler et al., 2005
Tis11		1	1	1	non-core	n.d.	Puig et al., 2005
Additional P proteins found in WT strain							
Dcp1	Dcp2, Edc1	1	3	3		Increased number when deleted alone, Smaller size in dcp1Δdcp2Δ	Dunckley and Parker, 1999, Borja et al., 2011,
Pby1	(Dcp1), (Edc3)	0	2	2		n.d.	Krogan et al., 2006,

1) Did not consider high-throughput studies

2) Unclear if interactions between Pat1 and Upf1 is direct. Demonstrated by two-hybrid assays.

3) Lsm4 valency is unclear

4) Interactions between Dhh1 and Pop2, Dhh1 and Eap1, and Eap1 and Smy2 were demonstrated by Co-IP, unclear if the interactions are direct.

5) Hek2 has 3 RNA binding KH domains, but whether all of them interact with RNA is unclear

6) Sbp1 has 2 RRM domains, not sure if they all interact with RNA.

7) For Edc1, in *dcp1*Δ strain, total number of interactions is 3 since Dcp1 is lacking.

8) Pby1 interacts with Dcp1 and Edc3 based on current dara, but it is unclear if the interactions are direct

Table 4. Plasmids used in this study

Plasmid name	description	makers	N-terminal tag	C-terminal tag	Notes
Dcp2 FL	carrying the *DCP2* promoter, a sequence encoding full length Dcp2 (1-970) - GFP and the *ADH1* terminator	amp+, -URA		GFP	
Dcp2 ΔN	carrying the *DCP2* promoter, a sequence encoding Dcp2 (243-970) - GFP and the *ADH1* terminator	amp+, -URA		GFP	
Dcp2 ΔH1	carrying the *DCP2* promoter, a sequence encoding Dcp2 (1-970) L255A - GFP and the *ADH1* terminator	amp+, -URA		GFP	
Dcp2 300	carrying the *DCP2* promoter, a sequence encoding Dcp2 (1-300) - GFP and the *ADH1* terminator	amp+, -URA		GFP	
Dcp2 300 ΔH1	carrying the *DCP2* promoter, a sequence encoding Dcp2 (1-300) L255A - GFP and the *ADH1* terminator	amp+, -URA		GFP	
Dcp2 300 AAAA	carrying the *DCP2* promoter, a sequence encoding Dcp2 (1-300) R170A K212A K216A R229A - GFP and the *ADH1* terminator	amp+, -URA		GFP	
Dcp2 ΔH1 WD	carrying the *DCP2* promoter, a sequence encoding Dcp2 (1-970) L255A W50A D54A- GFP and the *ADH1* terminator	amp+, -URA		GFP	
Dcp2C Δ5H	carrying the *DCP2* promoter, a sequence encoding Dcp2 (327-970) X440-450A X489-500A, X701-708A, X827-831A, X935-938A - GFP and the *ADH1* terminator	amp+, -URA		GFP	five Edc3 binding regions 440-450, 489-500, 701-708, 827-831, 935-938 were mutated to alanine
Dcp2 ΔH1 Δ5H	carrying the *DCP2* promoter, a sequence encoding Dcp2 (1-970) L255A X440-450A X489-500A, X701-708A, X827-831A, X935-938A - GFP and the *ADH1* terminator	amp+, -URA		GFP	five Edc3 binding regions 440-450, 489-500, 701-708, 827-831, 935-938 were mutated to alanine
Dcp2 FL-H1	carrying the *DCP2* promoter, a sequence encoding full length Dcp2 with Dcp2 amino acids 242-265 added after aa970 - GFP and the *ADH1* terminator	amp+, -URA		GFP	
Dcp2C Δ5H-H1	carrying the *DCP2* promoter, a sequence encoding Dcp2C Δ5H with Dcp2 amino acids 242-265 added after aa970- GFP and the *ADH1* terminator	amp+, -URA		GFP	
N-Dcp2	carrying the *DCP2* promoter, a sequence encoding GFP - Dcp2 (1-970) and the *ADH1* terminator	amp+, -URA	GFP		
Edc3	carrying the *EDC3* promoter, a sequence encoding Edc3-mCherry and the *EDC3* terminator	amp+, -LYS		mCherry	
Edc3	carrying the *EDC3* promoter, a sequence encoding Edc3-mCherry and the *EDC3* terminator	amp+, -TRP		mCherry	